

# EFFICIENT FINE-TUNING OF QUANTIZED MODELS VIA ADAPTIVE RANK AND BITWIDTH

**Anonymous authors**

Paper under double-blind review

## ABSTRACT

As large language models (LLMs) scale up, model compression is crucial for their deployment on resource-constrained devices. While methods like QLoRA reduce resource demands by combining parameter quantization with LoRA fine-tuning, their use of uniform precision can limit performance by failing to account for layer-wise variations in parameter sensitivity. Recent advances have explored dynamic mixed-precision quantization and adaptive LoRA ranks, but these strategies are typically optimized in isolation. The synergistic integration of these two dimensions remains an unresolved core challenge. To address this, we introduce **QR-Adaptor**, a unified, gradient-free framework that jointly optimizes the per-layer quantization bit-width and LoRA rank. Instead of indirectly minimizing quantization error, QR-Adaptor formulates the task as a discrete, multi-objective optimization problem, directly guided by downstream task performance and memory constraints using a small calibration dataset. Our extensive experiments show that QR-Adaptor consistently establishes a new Pareto frontier, outperforming state-of-the-art quantized fine-tuning methods. Notably, our approach can surpass the performance of a 16-bit LoRA fine-tuned model while operating with a memory footprint comparable to 4-bit models.

## 1 INTRODUCTION

Large Language Models (LLMs) have achieved remarkable success in both language understanding and generation (Makridakis et al., 2023; Raiaan et al., 2024; Chang et al., 2024). However, adapting these powerful models to specific downstream tasks is often hindered by immense computational and memory costs (Wan et al., 2023). Parameter-Efficient Fine-Tuning (PEFT) methods, such as Low-Rank Adaptation (LoRA) (Hu et al., 2022), address these bottlenecks by introducing lightweight updates, while quantization techniques (Gong et al., 2014; Gupta et al., 2015) compress model weights to fewer bits. Building on these two lines of research, QLoRA (Dettmers et al., 2023) has become a standard paradigm for memory-efficient LLM fine-tuning by integrating a 4-bit quantized base model with LoRA updates.

While effective, the static nature of QLoRA (i.e., uniform 4-bit quantization and a fixed LoRA rank) has motivated several lines of research seeking further improvements. One direction focuses on quantization, employing mixed-precision strategies to assign more bits to sensitive layers (e.g., MixLLM (Wang et al., 2025), Slim-LLM (Huang et al., 2025)). Another direction targets adaptation, with methods like AdaLoRA (Zhang et al., 2023b) dynamically allocating LoRA rank based on parameter importance. A third approach, exemplified by LoftQ (Li et al., 2023), focuses on better initializing LoRA matrices to compensate for quantization error. While valuable, these approaches tackle the problem from a single dimension—either bits, rank, or initialization—but overlook their potential interplay. This leaves a critical question unanswered: **how to holistically allocate a model’s limited memory budget between numerical precision (bit-width) and adaptive capacity (rank) on a per-layer basis?**

To bridge this gap, we introduce **QR-Adaptor**, the first framework to address the joint, discrete optimization of per-layer bit-widths and LoRA ranks. We posit that treating this as a unified search problem allows for a more effective allocation of resources. For instance, some layers may preserve functionality better with higher precision, while others might benefit more from increased adaptive capacity via a larger rank. QR-Adaptor directly navigates this trade-off by framing it as a multi-

**Table 1:** Comparison of our QR-Adaptor with existing methods for efficient LLM fine-tuning.

Method	Adaptation Strategy	Quantization Strategy	Joint Optimization?	Optimization Space
QLoRA (Detmers et al., 2023)	Static Rank (Uniform)	Static Bit-width (Uniform)	No	-
AdaLoRA (Zhang et al., 2023b)	Dynamic Rank (Per-layer)	Static Bit-width	No (Rank only)	Continuous
MixLLM/SHIM-LLM (Wang et al., 2025; Huang et al., 2025)	N/A (PTQ only)	Dynamic Bit-width (Per-layer)	No (Bits only)	Discrete
LoftQ (Li et al., 2023)	Static Rank (SVD-init)	Static Bit-width	Indirectly	Continuous
<b>QR-Adaptor (Ours)</b>	<b>Dynamic Rank (Per-layer)</b>	<b>Dynamic Bit-width (Per-layer)</b>	<b>Yes (Unified Search)</b>	<b>Discrete</b>

objective optimization task: maximizing downstream task performance while minimizing memory footprint. To solve this efficiently, our method employs a gradient-free search pipeline on a small calibration dataset, directly optimizing for the final task objective rather than relying on proxy metrics like quantization error.

To robustly navigate this high-dimensional discrete configuration space, QR-Adaptor adopts a three-stage optimization pipeline. It begins with a **task-informed initialization** that estimates layer importance, followed by a **global exploration** using a Pareto-ranking genetic algorithm to identify a diverse set of promising candidates. Finally, it conducts **local refinement** using Bayesian optimization to pinpoint the optimal configuration. This systematic approach allows QR-Adaptor to find superior configurations in the vast search space of bit-width and rank combinations. Our main contributions are as follows:

- We formulate the efficient fine-tuning of quantized LLMs as a **joint, multi-objective optimization problem**, considering per-layer bit-width and LoRA rank as coupled variables. This new perspective moves beyond the prevailing single-dimension optimization approaches.
- We propose **QR-Adaptor**, a novel and practical gradient-free framework to solve this problem. It efficiently searches the discrete configuration space using a combination of task-informed initialization, genetic algorithms, and Bayesian optimization.
- Through extensive experiments, we demonstrate that QR-Adaptor significantly advances the state-of-the-art. It establishes a superior **Pareto frontier** for the accuracy-memory trade-off and, in some cases, surpasses the performance of 16-bit LoRA fine-tuning with a memory footprint comparable to 4-bit models.

## 2 BACKGROUND AND MOTIVATION

To motivate our work, we first establish the necessity of a heterogeneous, per-layer approach for both quantization and parameter-efficient fine-tuning. We then discuss the limitations of existing methods that rely on continuous proxies to solve the inherently discrete problem of quantization-aware adaptation, paving the way for our proposed discrete search framework.

### 2.1 THE NEED FOR LAYER-WISE HETEROGENEITY

A core assumption in methods like QLoRA is uniformity: all adaptable layers are assigned the same quantization bit-width and LoRA rank. However, extensive research has shown that Large Language Models exhibit significant **layer-wise heterogeneity**, where different layers possess distinct properties and sensitivities.

**Sensitivity to Quantization.** It is well-documented that not all layers in an LLM are equally sensitive to the perturbations introduced by quantization. Seminal works in post-training quantization (PTQ), such as AWQ (Lin et al., 2023) and SmoothQuant (Xiao et al., 2022), identify that certain "outlier" features, often concentrated in specific layers, are critical for model performance. Consequently, applying a uniform low bit-width across the entire model can disproportionately harm these sensitive layers. This has led to the development of mixed-precision quantization schemes (Wang et al., 2025; Huang et al., 2025) that allocate more bits to more sensitive layers, thereby achieving a better balance between compression and accuracy.

**Sensitivity to Task Adaptation.** Similarly, during fine-tuning, layers contribute unequally to adapting the model to a new downstream task. The core idea behind methods like AdaLoRA (Zhang et al., 2023b) and RankAdaptor (Zhou et al., 2025) is to dynamically allocate more rank (i.e., more

trainable parameters) to layers whose weight updates are more significant for the task at hand. This demonstrates that a one-size-fits-all rank allocation is suboptimal for maximizing adaptation capacity under a fixed parameter budget.

**The Unaddressed Interplay.** These two lines of research highlight a critical, yet largely unaddressed, trade-off. For a given layer, how should a limited budget be allocated between **numerical precision (bit-width)** and **adaptive capacity (rank)**? For instance, for a layer identified as sensitive, is it more effective to increase its bit-width to preserve its original function, or to assign it a higher rank to allow it to better compensate for quantization effects during fine-tuning? Existing methods optimize these two dimensions in isolation. This motivates the need for a unified framework that can holistically solve this joint optimization problem on a per-layer basis.

## 2.2 LIMITATIONS OF CONTINUOUS PROXIES FOR A DISCRETE PROBLEM

Another line of work, such as LoftQ (Li et al., 2023), attempts to improve upon QLoRA by initializing the LoRA matrices ( $\mathbf{A}$  and  $\mathbf{B}$ ) to better compensate for the quantization error, typically by minimizing the Frobenius norm of the residual:

$$\min_{\mathbf{A}, \mathbf{B}} \|(\mathbf{W} - \text{Quantize}(\mathbf{W})) - \mathbf{A}\mathbf{B}\|_F. \quad (1)$$

While intuitive, this approach relies on a continuous proxy objective (the Frobenius norm) to address an inherently discrete problem. The fundamental challenge is that the target space for the quantized weights is a discrete lattice  $\Lambda = \Delta \cdot \mathbb{Z}^{d \times k}$ . A continuous low-rank update  $\mathbf{A}\mathbf{B}$  added to a quantized matrix  $\mathbf{Q} = \text{Quantize}(\mathbf{W})$  results in a matrix  $\mathbf{Q} + \mathbf{A}\mathbf{B}$  that almost certainly lies outside this lattice. To be used in the model, it must be re-quantized, i.e., projected back onto  $\Lambda$ .

This two-step process—continuous fitting followed by discrete projection—can be suboptimal. As we formalize in Appendix C, even the optimal continuous low-rank correction  $\mathbf{A}\mathbf{B}^*$  does not guarantee that the final quantized matrix  $\mathcal{P}_\Lambda(\mathbf{Q} + \mathbf{A}\mathbf{B}^*)$  is the best possible approximation of the original weight matrix  $\mathbf{W}$ . There often exists another discrete matrix  $\mathbf{Q}' \in \Lambda$  that is a better representation, but which is inaccessible via this indirect, residual-fitting procedure.

This observation motivates a paradigm shift: instead of indirectly minimizing a continuous error metric, a more direct and effective approach is to **search within the discrete configuration space itself**, using the final downstream task performance as the direct optimization signal. This is the core principle behind our proposed QR-Adaptor.

## 3 QR-ADAPTOR: A MULTI-STAGE FRAMEWORK FOR JOINT OPTIMIZATION

### 3.1 A MULTI-OBJECTIVE FORMULATION FOR QUANTIZED ADAPTATION

We frame the challenge of efficient LLM fine-tuning as a multi-objective optimization problem. For a model with  $L$  layers, our goal is to find an optimal configuration  $C = \{(q_l, r_l)\}_{l=1}^L$ , where  $q_l \in \mathcal{Q}$  is the quantization bit-width and  $r_l \in \mathcal{R}$  is the LoRA rank for layer  $l$ . The sets  $\mathcal{Q}$  (e.g.,  $\{2, 4, 8\}$ ) and  $\mathcal{R}$  (e.g.,  $\{4, 8, 16\}$ ) define the discrete search space.

The forward pass for a layer  $l$  with configuration  $(q_l, r_l)$  is given by:

$$\mathbf{y} = \text{Quantize}(\mathbf{W}_l, q_l) \cdot \mathbf{x} + \mathbf{A}_l \mathbf{B}_l \cdot \mathbf{x}, \quad (2)$$

where  $\mathbf{A}_l \in \mathbb{R}^{d \times r_l}$  and  $\mathbf{B}_l \in \mathbb{R}^{r_l \times k}$  are the LoRA matrices.

We aim to find a configuration  $C$  that simultaneously maximizes the model’s performance on a downstream task, denoted  $P(C)$ , and minimizes its memory footprint,  $M(C)$ . This defines a search for the Pareto optimal set  $\mathcal{C}^*$  in the solution space  $\mathcal{C}$ :

$$\mathcal{C}^* = \arg \min_{C \in \mathcal{C}} (-P(C), M(C)). \quad (3)$$

Since evaluating each candidate  $C$  requires a non-trivial fine-tuning process, this problem constitutes an expensive, black-box, multi-objective optimization over a high-dimensional, discrete space.

**Algorithm 1** The QR-Adaptor Framework

---

```

162 1: Input: Pre-trained model  $\mathcal{M}$ , calibration data  $\mathcal{D}_{\text{calib}}$ , search spaces  $\mathcal{Q}, \mathcal{R}$ .
163 2: Output: An optimal configuration  $C^* = \{(q_i^*, r_i^*)\}_{i=1}^L$ .
164
165   # Stage 1: Task-Informed Initialization
166 3: Compute layer importance scores  $\{I(l)\}_{l=1}^L$  using an entropy-based criterion on  $\mathcal{D}_{\text{calib}}$ .
167 4: Generate an initial seed configuration  $C_0$  based on importance scores.
168 5: Create an initial population  $\mathcal{P}_0$  by introducing perturbations around  $C_0$ .
169
170   # Stage 2: Global Exploration with PRGA
171 6: Initialize population with  $\mathcal{P}_0$ .
172 7:
173 8: for  $g = 1$  to  $G_{\text{max}}$  do
174 9:   Evaluate each configuration  $C \in \mathcal{P}_{g-1}$  on  $\mathcal{D}_{\text{calib}}$  to get  $(P(C), M(C))$ .
175 10:  Generate offspring population  $\mathcal{P}'_g$  via selection, crossover, and mutation.
176 11:  Select the next generation  $\mathcal{P}_g$  using Pareto ranking and crowding distance.
177 12: end for
178 13: Obtain the final Pareto front  $\mathcal{C}_{\text{pareto}}$  from  $\mathcal{P}_{G_{\text{max}}}$ .
179
180   # Stage 3: Local Refinement with Bayesian Optimization
181 14: Define a scalarized objective  $f(C) = \alpha P(C) - (1 - \alpha)M(C)$  with user preference  $\alpha$ .
182 15: Build a Gaussian Process surrogate model of  $f(C)$  using samples from  $\mathcal{C}_{\text{pareto}}$ .
183 16:
184 17: for  $t = 1$  to  $T_{\text{max}}$  do
185 18:   Select next candidate  $C_{t+1}$  by maximizing the Expected Improvement (EI) acquisition
186 19:   function.
187 19:   Evaluate  $f(C_{t+1})$  and update the surrogate model.
188 20: end for
189 21: return The best configuration found  $C^* = \arg \max_C f(C)$ .

```

---

## 3.2 THE QR-ADAPTOR SEARCH PIPELINE

The entire three-stage pipeline is designed to efficiently navigate the vast and discrete configuration space. Navigating this complex search space requires a specialized strategy. A purely random search would be inefficient, while methods relying on gradients are inapplicable. We therefore propose **QR-Adaptor**, a principled, three-stage search pipeline designed to efficiently identify near-optimal configurations. The pipeline orchestrates three well-established optimization techniques:

1. **Task-Informed Initialization:** An efficient heuristic to identify a promising region of the search space.
2. **Global Exploration with PRGA:** A genetic algorithm to broadly explore this region and identify the Pareto front.
3. **Local Refinement with Bayesian Optimization:** A sample-efficient method to fine-tune solutions along the Pareto front according to specific user preferences.

A detailed breakdown of the search hyperparameters, search spaces, and a step-by-step algorithm for the task-informed initialization stage is provided in Appendix E. The entire search process is conducted on a small calibration subset of the training data to keep the computational overhead manageable. The overall procedure is summarized in Algorithm 1.

## 3.2.1 STAGE 1: TASK-INFORMED INITIALIZATION

To avoid a blind start, we first estimate each layer’s importance using an information-theoretic criterion based on mutual information:

$$I(l) = H(Y) - H(Y|X_l), \quad (4)$$

where  $Y$  is the model’s output distribution and  $X_l$  is the representation at layer  $l$ , both estimated on  $\mathcal{D}_{\text{calib}}$ . Layers with higher  $I(l)$  have greater influence. We then generate a seed configuration  $C_0$  by allocating higher bit-widths and ranks to more important layers. An initial population  $\mathcal{P}_0$  for the

**Algorithm 2** Pareto Ranking Genetic Algorithm (PRGA)

---

```

216 1: Input: Initial population  $\mathcal{P}_0$ , calibration data  $\mathcal{D}_{\text{calib}}$ .
217 2: Output: Pareto front  $\mathcal{C}_{\text{pareto}}$ .
218 3: Evaluate fitness  $(-P(C), M(C))$  for all  $C \in \mathcal{P}_0$  on  $\mathcal{D}_{\text{calib}}$ .
219 4:  $(\mathcal{F}_1, \mathcal{F}_2, \dots) \leftarrow \text{Non-Dominated-Sort}(\mathcal{P}_0)$ .
220 5:
221 6: for  $g = 0$  to  $G_{\text{max}} - 1$  do
222 7:    $\mathcal{Q}_g \leftarrow \text{Create-Offspring}(\mathcal{P}_g)$  ▷ Tournament Selection, Crossover, Mutation
223 8:   Evaluate fitness for all  $C \in \mathcal{Q}_g$ .
224 9:    $\mathcal{R}_g \leftarrow \mathcal{P}_g \cup \mathcal{Q}_g$ .
225 10:   $(\mathcal{F}_1, \mathcal{F}_2, \dots) \leftarrow \text{Non-Dominated-Sort}(\mathcal{R}_g)$ .
226 11:   $\mathcal{P}_{g+1} \leftarrow \emptyset$ .
227 12:   $i \leftarrow 1$ .
228 13:  while  $|\mathcal{P}_{g+1}| + |\mathcal{F}_i| \leq |\mathcal{P}_0|$  do
229 14:     $\mathcal{P}_{g+1} \leftarrow \mathcal{P}_{g+1} \cup \mathcal{F}_i$ .
230 15:     $i \leftarrow i + 1$ .
231 16:  end while
232 17:  Crowding-Distance-Assignment( $\mathcal{F}_i$ ).
233 18:  Sort  $\mathcal{F}_i$  by descending crowding distance.
234 19:   $\mathcal{P}_{g+1} \leftarrow \mathcal{P}_{g+1} \cup \mathcal{F}_i[1 : (|\mathcal{P}_0| - |\mathcal{P}_{g+1}|)]$ .
235 20: end for
236 21: return The first Pareto front  $\mathcal{F}_1$  from the final population  $\mathcal{P}_{G_{\text{max}}}$ .

```

---

next stage is created by applying small, random perturbations to  $C_0$ , focusing search on a promising region.

### 3.2.2 STAGE 2: GLOBAL EXPLORATION WITH PRGA

With a promising initial population, we perform a global search using a Pareto Ranking Genetic Algorithm (PRGA), inspired by NSGA-II (Deb et al., 2002). The goal is to discover the Pareto frontier  $\mathcal{C}_{\text{pareto}}$ . The core logic is detailed in Algorithm 2. The algorithm iteratively evolves a population of configurations through selection, crossover, and mutation. Selection is guided by two principles: Pareto dominance (solutions on better fronts are preferred) and crowding distance (solutions in sparser regions of a front are preferred to maintain diversity). Crossover and mutation operators are adapted from Simulated Binary Crossover (SBX) and Polynomial Mutation to operate on the integer-pair representation of configurations. The visual flowchart is in Figure 3 in the Appendix

### 3.2.3 STAGE 3: LOCAL REFINEMENT WITH BAYESIAN OPTIMIZATION

The Pareto front from PRGA provides a set of excellent trade-off solutions. To pinpoint a single optimal configuration based on specific user preferences (e.g., maximizing performance under a strict memory budget), we employ Bayesian Optimization (BO).

First, we transform the multi-objective problem into a single-objective one by defining a scalarized objective function with a trade-off parameter  $\alpha \in [0, 1]$ :

$$\max_{C \in \mathcal{C}} f(C) = \alpha \cdot \text{norm}(P(C)) - (1 - \alpha) \cdot \text{norm}(M(C)). \quad (5)$$

We use the solutions on the Pareto front to build a Gaussian Process (GP) surrogate model for the expensive function  $f(C)$ . The GP provides a posterior distribution over the objective function for any candidate configuration  $C^*$ , characterized by its mean and variance:

$$\begin{aligned} \mu(C^*) &= \mathbf{k}_*^T (\mathbf{K} + \sigma_n^2 \mathbf{I})^{-1} \mathbf{y} \\ \sigma^2(C^*) &= k(C^*, C^*) - \mathbf{k}_*^T (\mathbf{K} + \sigma_n^2 \mathbf{I})^{-1} \mathbf{k}_*, \end{aligned} \quad (6)$$

where  $\mathbf{K}$  is the kernel matrix of the observed points,  $\mathbf{k}_*$  is the vector of covariances between  $C^*$  and observed points, and  $\mathbf{y}$  are the observed function values.

We then iteratively select the next configuration to evaluate by maximizing the Expected Improvement (EI) acquisition function. EI quantifies the expected amount of improvement over the current best

**Table 2:** Performance comparison of different methods across various bit-width configurations on LLaMa3.1-8B. Superscripts on LoftQ bits indicate the number of initialization iterations. Bold figures represent the best performance, while underlined figures indicate the second-best. Accuracy is reported as %.

Method	Bit	ARC(C)	ARC(E)	BoolQ	GSM8K	HellaS	OBQA	PIQA	WinoG	Average
LoRA	16	56.14	<u>83.88</u>	<u>83.18</u>	<u>54.36</u>	79.44	45.20	<u>82.10</u>	<b>75.30</b>	<u>69.95</u>
QLoRA	8	<b>57.08</b>	83.46	82.48	53.75	<u>79.63</u>	<b>46.00</b>	<u>82.10</u>	74.59	69.89
QLoRA	4	54.35	82.41	82.08	44.35	78.82	44.20	81.50	73.64	67.67
AdaLoRA	16	52.90	81.99	81.87	50.57	78.65	45.00	81.34	73.95	68.28
AdaLoRA	8	52.90	81.86	82.05	49.96	78.65	44.80	81.34	74.43	68.25
AdaLoRA	4	51.28	80.98	80.61	37.83	77.36	42.80	80.74	72.53	65.51
LoftQ	4 <sup>1</sup>	54.86	82.74	82.26	51.40	78.65	<b>46.00</b>	81.45	73.24	68.82
LoftQ	4 <sup>5</sup>	52.65	81.82	81.53	39.65	78.50	43.40	81.39	72.69	66.45
LoftQ	4 <sup>10</sup>	51.88	81.31	79.66	38.44	78.01	43.20	81.12	71.98	65.70
QuaRot	4	54.12	82.15	81.92	50.21	78.45	45.20	81.32	73.01	68.30
SpinQuant	4	54.45	82.32	82.05	51.03	78.62	45.60	81.41	73.15	68.58
QR-Adaptor ( $\leq 4$ -bit)	3.625	56.15	82.78	82.45	54.12	79.58	45.60	82.12	75.01	69.73
QR-Adaptor (Optimal)	5.45	<u>56.83</u>	<b>84.12</b>	<b>83.38</b>	<b>56.29</b>	<b>80.93</b>	<u>45.80</u>	<b>82.92</b>	<u>75.10</u>	<b>70.67</b>
ApiQ	2	48.12	76.45	75.32	28.45	72.15	38.20	75.67	65.89	62.53
RILQ	2	48.78	76.98	75.89	29.45	72.78	38.80	76.12	66.45	63.16
QR-Adaptor (Fixed 2-bit)	2	49.12	77.12	76.01	30.12	73.01	39.00	76.23	66.89	63.44
QR-Adaptor (Mixed 2/4-bit)	2.5	50.23	78.01	76.89	31.45	73.89	39.80	77.12	67.78	64.40
LoRA	16	<u>56.74</u>	<u>83.63</u>	<u>83.00</u>	<u>54.13</u>	<u>79.51</u>	44.40	<u>81.83</u>	74.43	69.70
QLoRA	8	56.23	82.91	82.66	53.68	79.46	<b>46.00</b>	81.66	<u>74.74</u>	69.67
QLoRA	4	53.84	81.99	82.11	44.66	78.76	44.40	81.72	73.09	67.57
AdaLoRA	16	53.07	82.03	81.99	50.11	78.61	45.40	81.28	74.11	68.33
AdaLoRA	8	53.33	82.03	82.11	49.13	78.57	45.20	81.34	73.79	68.19
AdaLoRA	4	50.85	80.72	80.73	37.98	77.34	42.80	80.52	73.16	65.51
LoftQ	4 <sup>1</sup>	55.12	82.58	82.69	49.81	78.82	<u>45.80</u>	81.28	74.27	68.80
LoftQ	4 <sup>5</sup>	53.92	82.32	81.56	42.00	78.54	43.80	81.56	72.77	67.06
LoftQ	4 <sup>10</sup>	52.90	81.69	81.56	39.88	78.64	43.80	81.07	71.98	66.44
QuaRot	4	54.23	82.28	82.01	50.89	78.58	45.20	81.45	73.18	68.48
SpinQuant	4	54.52	82.45	82.15	51.28	78.74	45.60	81.56	73.32	68.70
QR-Adaptor ( $\leq 4$ -bit)	3.625	56.15	82.78	82.45	54.12	79.58	45.60	82.12	75.01	69.73
QR-Adaptor (Optimal)	5.45	<b>56.83</b>	<b>84.12</b>	<b>83.38</b>	<b>56.29</b>	<b>80.93</b>	<u>45.80</u>	<b>82.92</b>	<b>75.10</b>	<b>70.67</b>

observed value  $f(C^+)$ , balancing exploration and exploitation:

$$\begin{aligned}
 \text{EI}(C^*) &= (\mu(C^*) - f(C^+))\Phi(Z) + \sigma(C^*)\phi(Z) \\
 \text{with } Z &= \frac{\mu(C^*) - f(C^+)}{\sigma(C^*)},
 \end{aligned} \tag{7}$$

where  $\Phi(\cdot)$  and  $\phi(\cdot)$  are the CDF and PDF of the standard normal distribution. This sample-efficient process allows us to quickly converge on a refined optimal solution  $C^*$  that best satisfies the user-defined preference  $\alpha$ . The visual flowchart is in Figure 4 in the Appendix

## 4 EVALUATION

In this section, we first introduce the experimental setup, including datasets, models, baselines, and implementation details. All hyperparameters aside from rank value and bit-width are kept consistent with the baselines.

### 4.1 EXPERIMENTAL SETUP

**Datasets and LLMs.** We utilize the Alpaca52k and hc3 (Taori et al., 2023) for fine-tuning and evaluate the zero-shot performance of these LLMs on benchmarks including BoolQ (Clark et al., 2019), PIQA (Bisk et al., 2020), HellaSwag (Zellers et al., 2019), WinoGrande (Sakaguchi et al., 2021), ARC-easy (Clark et al., 2018), ARC-challenge (Clark et al., 2018), OpenbookQA (Mihaylov et al., 2018), and MMLU Hendrycks et al. (2021). The models used in our experiments are LLaMA2 Touvron et al. (2023), LLaMA3.1 Grattafiori et al. (2024), LLaMA3.2, and Qwen2.5 Qwen et al. (2025). These models cover a range of scales and architectures to demonstrate the generalizability of our approach across different model families.

**Baselines.** We compare our method against several baselines: without tuning, LoRA Hu et al. (2022), QLoRA Dettmers et al. (2023), Adalora Zhang et al. (2023b), LoftQ Li et al. (2023), and

**Table 3:** Performance comparison across different model architectures ( $r=8$ ). Bold figures represent the best performance for each model. Accuracy is reported as %.

Model	Method	Bit	ARC(C)	ARC(E)	BoolQ	GSM8K	HellaS	OBQA	PIQA	WinoG	Average
Qwen-2.5-7B	LoRA	16	56.01	83.48	82.97	54.03	79.01	45.00	81.95	74.98	69.68
	QLoRA	4	54.02	82.04	81.53	44.11	78.02	44.00	81.04	72.96	67.22
	AdaLoRA	4	51.03	80.51	80.04	37.23	77.04	42.60	80.53	72.01	65.11
	LoftQ	4 <sup>1</sup>	53.96	82.15	81.87	43.84	77.93	43.80	80.72	72.54	67.11
	QR-Adaptor ( $\leq 4$ bit)	3.875	54.89	82.71	82.25	49.87	78.73	45.20	81.49	73.40	68.56
	QR-Adaptor (Optimal)	5.125	<b>56.52</b>	<b>84.01</b>	<b>83.49</b>	<b>56.03</b>	<b>80.52</b>	<b>46.00</b>	<b>82.51</b>	<b>75.52</b>	<b>70.58</b>
Qwen-2.5-3B	LoRA	16	52.98	81.03	80.01	45.02	76.01	42.00	79.03	70.99	65.88
	QLoRA	4	51.01	79.02	79.03	36.04	75.01	41.00	78.02	68.97	63.51
	AdaLoRA	4	49.03	78.01	78.02	29.01	74.03	40.00	77.01	68.03	61.64
	LoftQ	4 <sup>1</sup>	50.92	79.23	78.87	35.48	74.95	40.60	77.87	68.65	63.32
	QR-Adaptor ( $\leq 4$ bit)	3.375	51.87	79.91	79.76	41.03	75.45	41.80	78.43	69.41	64.69
	QR-Adaptor (Optimal)	4.875	<b>53.53</b>	<b>81.51</b>	<b>80.52</b>	<b>47.01</b>	<b>77.03</b>	<b>43.00</b>	<b>79.51</b>	<b>71.52</b>	<b>66.70</b>
LLaMA-3.2-3B	LoRA	16	53.51	81.23	80.51	46.03	76.51	42.60	79.52	71.31	66.39
	QLoRA	4	51.52	79.51	79.52	37.01	75.53	41.60	78.53	69.51	64.08
	AdaLoRA	4	49.53	78.52	78.51	30.03	74.52	40.60	77.51	68.52	62.21
	LoftQ	4 <sup>1</sup>	51.78	79.83	79.87	37.42	75.78	41.20	78.72	69.84	64.49
	QR-Adaptor ( $\leq 4$ bit)	3.75	52.41	80.25	80.17	42.01	75.95	42.20	78.96	69.95	65.23
	QR-Adaptor (Optimal)	5.375	<b>54.01</b>	<b>81.83</b>	<b>81.02</b>	<b>48.01</b>	<b>77.52</b>	<b>43.60</b>	<b>80.01</b>	<b>72.03</b>	<b>67.24</b>

LQ-LoRA Guo et al. (2024). We evaluated the performance of LoftQ with different iteration numbers. For Adalora, which dynamically allocates ranks based on the average rank budget, we set the budget to 8 and 64. Finally, for LQ-LoRA, which allocates quantization bit-width based on the average weight bit-width budget and quantization error, we set the bit-width budget to 4. Additionally, we include recent 4-bit quantization methods: QuaRot Ashkboos et al. (2024), which uses random rotations to handle outliers, and SpinQuant Liu et al. (2024b), which employs learned rotations for optimal quantization accuracy. For extreme low-bit comparison, we evaluate against 2-bit methods including ApiQ Liao et al. (2024) and RILQ Lee et al. (2025), both utilizing LoRA-based quantization error compensation.

**Implementation Details.** We utilize the following configurations: *PyTorch* version 2.1.2, *Bit-sandBytes* library version 0.43.1, *Transformers* library version 4.41.0, *PEFT* library version 0.11.1, *Optuna* library version 3.6.1, *CUDA* version 12.4, *GPU*: NVIDIA L20. *Operating System*: Ubuntu. Concise implementation details are provided in the Appendix I. We define the population size as 5 and generate 1 new offspring in each iteration. The second and third phases were iterated 5 times.

## 4.2 MAIN RESULTS

We present the performance comparison of LLaMA3.1-8B on commonsense understanding tasks in Table 2. We further evaluate QR-Adaptor on three additional models (Qwen-2.5-7B, Qwen-2.5-3B, and LLaMA-3.2-3B) as shown in Table 3. For practical deployment considerations, we include both  $\leq 4$ -bit constrained and optimal configurations. Our method achieves or surpasses the performance of 16-bit fine-tuned models while maintaining competitive memory usage.

As mentioned, LoftQ outperforms 4-bit QLoRA after one iteration, but its performance degrades with more iterations due to the mismatch between continuous error correction and discrete quantization. Recent 4-bit methods like QuaRot and SpinQuant, which use rotation-based outlier handling, show competitive results but still fall short of our approach. For extreme quantization, we compare against 2-bit methods including ApiQ and RILQ. QR-Adaptor demonstrates consistent improvements across all bit-width regimes.

QR-Adaptor jointly optimizes bit-width and LoRA rank, balancing precision and adaptation capacity for superior performance. Notably, even under strict  $\leq 4$ -bit constraints (average 3.625 bits), QR-Adaptor achieves 69.37% average accuracy, outperforming all 4-bit baselines. In the optimal configuration (5.45 bits average), it reaches 70.67%, substantially exceeding both traditional and recent quantization methods. Furthermore, QR-Adaptor allocates resources more efficiently by assigning higher LoRA ranks to critical layers and higher precision to important layers, achieving high accuracy with low memory usage.

Due to space constraints, additional experimental results and analyses are provided in Appendix G, including: (1) extended results across different models (G.1, G.2, G.5, G.6); (2) evaluations on larger datasets with higher LoRA ranks (G.3).

**Table 5:** Performance comparison of different methods across various bit-width configurations on Llama3.1-8B with higher ranks. Bold figures represent the best performance for a given model and task, while underlined figures indicate the second-best. QR-Adaptor\* is transferred config. Accuracy is reported as %.

Method	Rank	Bit	ARC(C)	ARC(E)	BoolQ	HellaS	OBQA	PIQA	WinoG	MMLU	Average
LoRA	32	16	54.86	82.74	82.75	<u>79.21</u>	44.40	<u>81.99</u>	74.11	63.66	70.47
LoRA	64	16	<u>55.46</u>	82.95	<u>82.94</u>	79.13	45.00	81.88	<u>74.51</u>	<u>64.34</u>	<u>70.78</u>
QLoRA	32	8	55.20	<u>83.12</u>	81.93	79.07	<b>46.20</b>	81.88	73.32	63.28	70.50
QLoRA	32	4	53.41	80.89	82.05	78.42	43.60	80.90	73.01	60.97	69.16
QLoRA	64	8	<u>55.46</u>	83.04	81.96	79.17	<u>45.80</u>	81.94	73.01	63.34	70.47
QLoRA	64	4	53.41	81.19	81.74	78.35	44.60	80.69	72.06	60.79	69.10
AdaLoRA	32	8	53.92	81.82	82.20	78.57	<b>46.20</b>	81.50	73.40	63.82	70.18
AdaLoRA	32	4	51.45	81.02	80.86	77.30	42.40	80.96	72.53	58.15	68.08
AdaLoRA	64	8	53.92	82.11	81.93	78.74	46.20	81.39	73.95	63.88	70.27
AdaLoRA	64	4	52.13	80.98	81.04	77.20	42.20	80.85	72.77	58.07	68.16
LoftQ	32	4 <sup>1</sup>	53.84	81.36	81.41	78.12	43.00	81.50	73.56	59.40	69.02
LoftQ	32	4 <sup>5</sup>	52.56	81.36	81.96	78.05	42.80	81.45	73.09	59.41	68.84
LoftQ	32	4 <sup>10</sup>	51.62	81.31	82.51	78.16	43.60	81.34	72.30	59.12	68.75
LoftQ	64	4 <sup>1</sup>	52.82	81.40	81.59	78.23	43.20	81.34	73.88	59.78	69.03
LoftQ	64	4 <sup>5</sup>	52.39	81.10	81.13	78.33	43.40	81.34	73.24	58.69	68.70
LoftQ	64	4 <sup>10</sup>	51.71	81.23	81.62	78.37	43.20	81.01	72.77	59.25	68.65
QR-Adaptor*	32	3.625	55.23	82.89	82.65	79.12	45.40	81.77	73.88	63.78	70.59
QR-Adaptor	32	5.875	<b>56.12</b>	<b>83.45</b>	<b>83.21</b>	<b>79.78</b>	<b>46.20</b>	<b>82.10</b>	<b>74.59</b>	<b>64.40</b>	<b>71.23</b>

### 4.3 COMPUTATIONAL EFFICIENCY

The computational cost of QR-Adaptor primarily stems from actual performance testing on calibration data during stages 2 and 3. Specifically, after predicting a configuration, we need to conduct real performance tests to validate predictions. The prediction process itself is extremely fast (second-level), while one performance test on LLaMA3.1-8B model requires approximately 8-9 minutes. In comparison, one LoftQ iteration takes 11 minutes, and AdaLoRA, due to its dynamic rank adjustment during training, is typically 30-35% slower than LoRA.

QR-Adaptor’s advantage becomes evident in resource-constrained scenarios where performance optimization is critical. While the initial search requires multiple performance evaluations, the method can continuously improve model performance through iterative optimization. Moreover, the three-stage design ensures efficient exploration of the configuration space, requiring fewer total evaluations compared to exhaustive search approaches.

To provide a comprehensive time comparison, we conducted experiments fine-tuning LLaMA3.1-8B on Alpaca52k dataset for 2 epochs across different methods. The results are summarized in Table 4.

To address potential concerns about computational overhead, we investigated the transferability of optimized configurations across datasets. We found that configurations optimized on one dataset exhibit significant transferability when applied to fine-tuning on different datasets. Specifically, when directly using a configuration optimized on dataset A for fine-tuning on dataset B, we still achieve notable performance improvements compared to baseline methods, albeit not as substantial as performing optimization specifically for dataset B.

As shown in Table 9, the "QR-Adaptor (Transferred Config)" row demonstrates the performance when directly applying a configuration optimized on a 52k dataset to the larger 177k dataset. This demonstrates that the same model’s optimized configurations possess transferability, enabling direct use in fine-tuning on different datasets while still achieving significant performance improvements.

**Table 4:** Training time comparison of different methods on LLaMA3.1-8B with Alpaca52k dataset (2 epochs). All experiments were conducted on L20 GPU.

Method	Total Time (minutes)
LoRA	300
QLoRA	360-405
AdaLoRA	390-405
LoftQ (1 iteration)	370-416
LoftQ (5 iterations)	415-460
LoftQ (10 iterations)	470-515
QR-Adaptor	445-495



#### 4.4 ABLATION STUDY

We use the WinoGrande benchmark to conduct an ablation study assessing the contribution of each stage in QR-Adaptor. As shown in Figure 1, removing either PRGA or Bayesian optimization leads to unbalanced search behavior—PRGA alone explores too broadly, while Bayesian optimization alone is overly narrow—reflecting their extrapolation and interpolation roles, respectively. Omitting stage 1 causes PRGA to initiate from random configurations, resulting in scattered search patterns. Nonetheless, it still reaches the upper-left optimal region, highlighting the strength of PRGA and Bayesian optimization. In contrast, the full three-stage pipeline first explores broadly around a guided initialization, then refines near promising areas, yielding the best configurations.

Further ablation studies assess the impact of each stage by removing them individually and analyzing the resulting performance. We also perform sensitivity analysis on PRGA hyperparameters, with details provided in Appendix J.

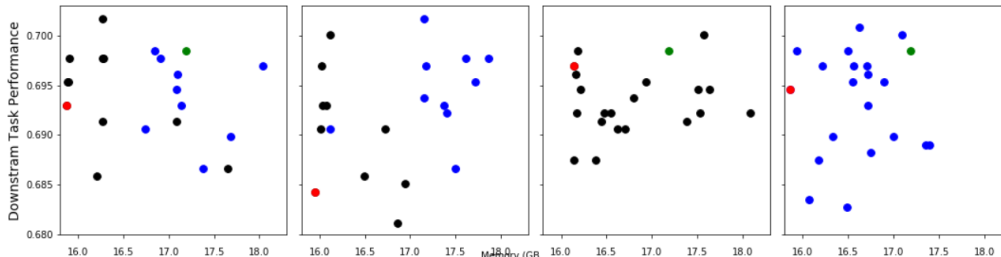


**Figure 1:** From left to right, the actual measured performance and memory usage of the configurations generated by QR-Adaptor, QR-Adaptor without stage1, QR-Adaptor without stage2, and QR-Adaptor without stage3 are shown. Different colors represent the configurations generated at different stages.

## 5 RELATED WORK

**LLM Quantization.** LLM quantization enables efficient deployment by reducing precision. Notable methods include GPTQ Frantar et al. (2023), AWQ Lin et al. (2023), SmoothQuant Xiao et al. (2023), ZeroQuant Yao et al. (2022), and LLM.int8() Dettmers et al. (2022). Mixed-precision approaches such as APTQ Guan et al. (2024), MixLLM Wang et al. (2025), and Slim-LLM Huang et al. highlight the importance of per-layer precision allocation, though they focus solely on quantization.

**Parameter Efficient Fine-Tuning.** PEFT methods enhance LLMs without heavy inference costs. QLoRA Dettmers et al. (2023) and LoftQ Li et al. (2023) combine quantization with low-rank adapters. Variants such as AdaLoRA Zhang et al. (2023a), LQ-LoRA Guo et al. (2023), RankAdaptor Zhou et al. (2024), and DoRA Liu et al. (2024a) emphasize adaptive allocation across layers, but remain independent of quantization.

**Joint Quantization and Low-Rank Adaptation.** LoftQ Li et al. (2023) alternates between quantization and low-rank approximation, while LQ-LoRA Guo et al. (2023) combines the two under memory constraints. However, existing approaches typically optimize quantization and adaptation separately, leaving joint allocation of precision and rank underexplored. More related work is in the Appendix A.

## 6 CONCLUSION

In this work, we propose QR-Adaptor, a unified, gradient-free method that uses partial calibration data to simultaneously optimize the precision and LoRA rank of each model layer. By focusing on the discrete nature of quantization and low-rank spaces and optimizing them within a task-driven framework, QR-Adaptor overcomes the limitations of iterative error-fitting techniques and rank-adaptive methods unsuitable for quantization. Our extensive experiments demonstrate that QR-Adaptor consistently outperforms existing baselines, achieving better performance than 16-bit fine-tuned models while maintaining a 4-bit memory footprint. These results highlight the importance of integrating quantization and low-rank matrices into a single, cohesive optimization process, driven by actual performance and memory efficiency.

## ETHICS STATEMENT

This work builds upon pre-trained large language models Llama2 and utilizes publicly available datasets for instruction fine-tuning Alpaca-clean. We do not introduce any new datasets or data collection processes, and therefore do not involve human annotation in this research. Additionally, our study focuses on improving model efficiency through pruning and quantization techniques, without engaging with sensitive content or user-specific data. As such, this paper does not present any ethical concerns beyond those already associated with the broader body of research on large language models and their datasets. All datasets and models used comply with their respective licenses and terms of use.

## REPRODUCIBILITY STATEMENT

To ensure the reproducibility of our results, we provide comprehensive documentation on the steps required to replicate our experiments. Our code is available in scripts such as `optuna_main-v3.py`, `post_training_mixed_quant.py`, and `run_optuna.py`, which handle hyperparameter optimization, mixed-precision quantization, and evaluation. For data preparation, we utilize the Alpaca Cleaned Dataset from `yahma/alpaca-cleaned`, which is automatically downloaded and processed using the `datasets` library. Our environment setup requires an NVIDIA GPU with CUDA support, preferably with at least 20 GB of memory for the Llama2 model, as well as Python 3.8+ and dependencies like PyTorch, Transformers, Optuna, BitsAndBytes, PEFT, and other libraries, which can be installed via the `requirements.txt` file. The model we fine-tune is the Llama2 architecture (NousResearch/Llama-2-7b-hf), using a mixed-precision quantization approach via `bitsandbytes` and Low-Rank Adaptation (LoRA) with the `peft` library. The training is conducted using a mixed-precision setup where the model's dtype is set to `torch.bfloat16` to optimize memory usage and computation efficiency. Our hyperparameter optimization framework leverages Optuna to maximize model accuracy while minimizing memory usage, tuning parameters like quantization bits (4 or 8 bits) and LoRA ranks (2 to 16). To replicate our training process, researchers can execute the provided scripts using the specified command-line arguments, which configure the model, output directories, number of trials, and evaluation tasks. Model checkpoints and Optuna results are saved at regular intervals. The training is conducted using the Hugging Face Trainer, configured with parameters including a batch size of 4, gradient accumulation steps of 16, warmup steps of 100, and a learning rate of  $1e-4$ , with evaluation and model saving steps set to every 200 steps. Evaluation is conducted using the `lm_eval` library, where metrics such as accuracy are recorded and saved in JSON format. All hyperparameter settings and model configurations are logged in the output directory, along with training progress and memory usage. Random seeds are set to ensure deterministic behavior. By following these steps, including hardware and software specifications, and running the scripts with the provided configurations, researchers can reproduce our experiments and validate the findings related to mixed-precision quantization and parameter-efficient fine-tuning.

## REFERENCES

- Saleh Ashkboos, Amirkeivan Mohtashami, Maximilian L Croci, Bo Li, Pashmina Cameron, Martin Jaggi, Dan Alistarh, Torsten Hoefer, and James Hensman. Quarot: Outlier-free 4-bit inference in rotated llms. *Advances in Neural Information Processing Systems*, 37:100213–100240, 2024.
- Jules Berman and Benjamin Peherstorfer. Colora: Continuous low-rank adaptation for reduced implicit neural modeling of parameterized partial differential equations, 2024. URL <https://arxiv.org/abs/2402.14646>.
- Yonatan Bisk, Rowan Zellers, Jianfeng Gao, Yejin Choi, et al. Piqa: Reasoning about physical commonsense in natural language. In *Proceedings of the AAAI conference on artificial intelligence*, volume 34, pp. 7432–7439, 2020.
- Yupeng Chang, Xu Wang, Jindong Wang, Yuan Wu, Linyi Yang, Kaijie Zhu, Hao Chen, Xiaoyuan Yi, Cunxiang Wang, Yidong Wang, et al. A survey on evaluation of large language models. *ACM Transactions on Intelligent Systems and Technology*, 15(3):1–45, 2024.

- 540 Christopher Clark, Kenton Lee, Ming-Wei Chang, Tom Kwiatkowski, Michael Collins, and Kristina  
541 Toutanova. Boolq: Exploring the surprising difficulty of natural yes/no questions. In *Proceedings*  
542 *of the 2019 Conference of the North American Chapter of the Association for Computational*  
543 *Linguistics: Human Language Technologies, Volume 1 (Long and Short Papers)*, pp. 2924–2936,  
544 2019.
- 545 Peter Clark, Isaac Cowhey, Oren Etzioni, Tushar Khot, Ashish Sabharwal, Carissa Schoenick, and  
546 Oyvind Tafjord. Think you have solved question answering? try arc, the ai2 reasoning challenge.  
547 *arXiv preprint arXiv:1803.05457*, 2018.
- 548 Kalyanmoy Deb, Amrit Pratap, Sameer Agarwal, and TAMT Meyarivan. A fast and elitist multiob-  
549 jective genetic algorithm: Nsga-ii. *IEEE transactions on evolutionary computation*, 6(2):182–197,  
550 2002.
- 551 Tim Dettmers, Mike Lewis, Younes Belkada, and Luke Zettlemoyer. Llm.int8(): 8-bit matrix  
552 multiplication for transformers at scale. *CoRR*, abs/2208.07339, 2022. URL <http://arxiv.org/abs/2208.07339>.
- 553 Tim Dettmers, Artidoro Pagnoni, Ari Holtzman, and Luke Zettlemoyer. Qlora: Efficient finetuning  
554 of quantized llms. *arXiv preprint arXiv:2305.14314*, 2023.
- 555 Elias Frantar, Sahar Ashkboos, Torsten Hoefler, and Dan Alistarh. Gptq: Accurate post-training  
556 quantization for generative pre-trained transformers. In *The Eleventh International Conference on*  
557 *Learning Representations (ICLR)*, 2023.
- 558 Yunchao Gong, Liu Liu, Ming Yang, and Lubomir Bourdev. Compressing deep convolutional  
559 networks using vector quantization. *arXiv preprint arXiv:1412.6115*, 2014.
- 560 Aaron Grattafiori, Abhimanyu Dubey, Abhinav Jauhri, Abhinav Pandey, Abhishek Kadian, Ahmad  
561 Al-Dahle, Aiesha Letman, Akhil Mathur, Alan Schelten, Alex Vaughan, Amy Yang, Angela Fan,  
562 Anirudh Goyal, Anthony Hartshorn, Aobo Yang, Archi Mitra, Archie Sravankumar, Artem Korenev,  
563 Arthur Hinsvark, Arun Rao, Aston Zhang, Aurelien Rodriguez, Austen Gregerson, Ava Spataru,  
564 Baptiste Roziere, Bethany Biron, Binh Tang, Bobbie Chern, Charlotte Caucheteux, Chaya Nayak,  
565 Chloe Bi, Chris Marra, Chris McConnell, Christian Keller, Christophe Touret, Chunyang Wu,  
566 Corinne Wong, Cristian Canton Ferrer, Cyrus Nikolaidis, Damien Allonsius, Daniel Song, Danielle  
567 Pintz, Danny Livshits, Danny Wyatt, David Esiobu, Dhruv Choudhary, Dhruv Mahajan, Diego  
568 Garcia-Olano, Diego Perino, Dieuwke Hupkes, Egor Lakomkin, Ehab AlBadawy, Elina Lobanova,  
569 Emily Dinan, Eric Michael Smith, Filip Radenovic, Francisco Guzmán, Frank Zhang, Gabriel  
570 Synnaeve, Gabrielle Lee, Georgia Lewis Anderson, Govind Thattai, Graeme Nail, Gregoire Mialon,  
571 Guan Pang, Guillem Cucurell, Hailey Nguyen, Hannah Korevaar, Hu Xu, Hugo Touvron, Iliyan  
572 Zarov, Imanol Arrieta Ibarra, Isabel Kloumann, Ishan Misra, Ivan Evtimov, Jack Zhang, Jade Copet,  
573 Jaewon Lee, Jan Geffert, Jana Vranes, Jason Park, Jay Mahadeokar, Jeet Shah, Jelmer van der Linde,  
574 Jennifer Billock, Jenny Hong, Jenya Lee, Jeremy Fu, Jianfeng Chi, Jianyu Huang, Jiawen Liu, Jie  
575 Wang, Jiecao Yu, Joanna Bitton, Joe Spisak, Jongsoo Park, Joseph Rocca, Joshua Johnstun, Joshua  
576 Saxe, Junteng Jia, Kalyan Vasuden Alwala, Karthik Prasad, Kartikeya Upasani, Kate Plawiak,  
577 Ke Li, Kenneth Heafield, Kevin Stone, Khalid El-Arini, Krithika Iyer, Kshitiz Malik, Kuenley  
578 Chiu, Kunal Bhalla, Kushal Lakhotia, Lauren Rantala-Yearry, Laurens van der Maaten, Lawrence  
579 Chen, Liang Tan, Liz Jenkins, Louis Martin, Lovish Madaan, Lubo Malo, Lukas Blecher, Lukas  
580 Landzaat, Luke de Oliveira, Madeline Muzzi, Mahesh Pasupuleti, Mannat Singh, Manohar Paluri,  
581 Marcin Kardas, Maria Tsimpoukelli, Mathew Oldham, Mathieu Rita, Maya Pavlova, Melanie  
582 Kambadur, Mike Lewis, Min Si, Mitesh Kumar Singh, Mona Hassan, Naman Goyal, Narjes  
583 Torabi, Nikolay Bashlykov, Nikolay Bogoychev, Niladri Chatterji, Ning Zhang, Olivier Duchenne,  
584 Onur Çelebi, Patrick Alrassy, Pengchuan Zhang, Pengwei Li, Petar Vasic, Peter Weng, Prajjwal  
585 Bhargava, Pratik Dubal, Praveen Krishnan, Punit Singh Koura, Puxin Xu, Qing He, Qingxiao Dong,  
586 Ragavan Srinivasan, Raj Ganapathy, Ramon Calderer, Ricardo Silveira Cabral, Robert Stojnic,  
587 Roberta Raileanu, Rohan Maheswari, Rohit Girdhar, Rohit Patel, Romain Sauvestre, Ronnie  
588 Polidoro, Roshan Sumbaly, Ross Taylor, Rui Hou, Rui Wang, Saghar Hosseini, Sahana  
589 Chennabasappa, Sanjay Singh, Sean Bell, Seohyun Sonia Kim, Sergey Edunov, Shaoliang Nie,  
590 Sharan Narang, Sharath Rapparthi, Sheng Shen, Shengye Wan, Shruti Bhosale, Shun Zhang, Simon  
591 Vandenhende, Soumya Batra, Spencer Whitman, Sten Sootla, Stephane Collot, Suchin Gururangan,  
592 Sydney Borodinsky, Tamar Herman, Tara Fowler, Tarek Sheasha, Thomas Georgiou, Thomas

594 Scialom, Tobias Speckbacher, Todor Mihaylov, Tong Xiao, Ujjwal Karn, Vedanuj Goswami,  
595 Vibhor Gupta, Vignesh Ramanathan, Viktor Kerkez, Vincent Gonguet, Virginie Do, Vish Vogeti,  
596 Vitor Albiero, Vladan Petrovic, Weiwei Chu, Wenhan Xiong, Wenyin Fu, Whitney Meers, Xavier  
597 Martinet, Xiaodong Wang, Xiaofang Wang, Xiaoqing Ellen Tan, Xide Xia, Xinfeng Xie, Xuchao  
598 Jia, Xuwei Wang, Yaelle Goldschlag, Yashesh Gaur, Yasmine Babaei, Yi Wen, Yiwen Song,  
599 Yuchen Zhang, Yue Li, Yuning Mao, Zacharie Delpierre Coudert, Zheng Yan, Zhengxing Chen, Zoe  
600 Papakipos, Aaditya Singh, Aayushi Srivastava, Abha Jain, Adam Kelsey, Adam Shajnfeld, Adithya  
601 Gangidi, Adolfo Victoria, Ahuva Goldstand, Ajay Menon, Ajay Sharma, Alex Boesenberg, Alexei  
602 Baevski, Allie Feinstein, Amanda Kallet, Amit Sangani, Amos Teo, Anam Yunus, Andrei Lupu,  
603 Andres Alvarado, Andrew Caples, Andrew Gu, Andrew Ho, Andrew Poulton, Andrew Ryan, Ankit  
604 Ramchandani, Annie Dong, Annie Franco, Anuj Goyal, Aparajita Saraf, Arkabandhu Chowdhury,  
605 Ashley Gabriel, Ashwin Bharambe, Assaf Eisenman, Azadeh Yazdan, Beau James, Ben Maurer,  
606 Benjamin Leonhardi, Bernie Huang, Beth Loyd, Beto De Paola, Bhargavi Paranjape, Bing Liu,  
607 Bo Wu, Boyu Ni, Braden Hancock, Bram Wasti, Brandon Spence, Brani Stojkovic, Brian Gamido,  
608 Britt Montalvo, Carl Parker, Carly Burton, Catalina Mejia, Ce Liu, Changan Wang, Changkyu  
609 Kim, Chao Zhou, Chester Hu, Ching-Hsiang Chu, Chris Cai, Chris Tindal, Christoph Feichtenhofer,  
610 Cynthia Gao, Damon Civin, Dana Beaty, Daniel Kreymer, Daniel Li, David Adkins, David Xu,  
611 Davide Testuggine, Delia David, Devi Parikh, Diana Liskovich, Didem Foss, Dingkan Wang, Duc  
612 Le, Dustin Holland, Edward Dowling, Eissa Jamil, Elaine Montgomery, Eleonora Presani, Emily  
613 Hahn, Emily Wood, Eric-Tuan Le, Erik Brinkman, Esteban Arcaute, Evan Dunbar, Evan Smothers,  
614 Fei Sun, Felix Kreuk, Feng Tian, Filippos Kokkinos, Firat Ozgenel, Francesco Caggioni, Frank  
615 Kanayet, Frank Seide, Gabriela Medina Florez, Gabriella Schwarz, Gada Badeer, Georgia Swee,  
616 Gil Halpern, Grant Herman, Grigory Sizov, Guangyi, Zhang, Guna Lakshminarayanan, Hakan Inan,  
617 Hamid Shojanazeri, Han Zou, Hannah Wang, Hanwen Zha, Haroun Habeeb, Harrison Rudolph,  
618 Helen Suk, Henry Aspegren, Hunter Goldman, Hongyuan Zhan, Ibrahim Damlaj, Igor Molybog,  
619 Igor Tufanov, Ilias Leontiadis, Irina-Elena Veliche, Itai Gat, Jake Weissman, James Geboski, James  
620 Kohli, Janice Lam, Japhet Asher, Jean-Baptiste Gaya, Jeff Marcus, Jeff Tang, Jennifer Chan, Jenny  
621 Zhen, Jeremy Reizenstein, Jeremy Teboul, Jessica Zhong, Jian Jin, Jingyi Yang, Joe Cummings,  
622 Jon Carvill, Jon Shepard, Jonathan McPhie, Jonathan Torres, Josh Ginsburg, Junjie Wang, Kai  
623 Wu, Kam Hou U, Karan Saxena, Kartikay Khandelwal, Katayoun Zand, Kathy Matosich, Kaushik  
624 Veeraraghavan, Kelly Michelena, Keqian Li, Kiran Jagadeesh, Kun Huang, Kunal Chawla, Kyle  
625 Huang, Lailin Chen, Lakshya Garg, Lavender A, Leandro Silva, Lee Bell, Lei Zhang, Liangpeng  
626 Guo, Licheng Yu, Liron Moshkovich, Luca Wehrstedt, Madian Khabza, Manav Avalani, Manish  
627 Bhatt, Martynas Mankus, Matan Hasson, Matthew Lennie, Matthias Reso, Maxim Groshev, Maxim  
628 Naumov, Maya Lathi, Meghan Keneally, Miao Liu, Michael L. Seltzer, Michal Valko, Michelle  
629 Restrepo, Mihir Patel, Mik Vyatskov, Mikayel Samvelyan, Mike Clark, Mike Macey, Mike Wang,  
630 Miquel Jubert Hermoso, Mo Metanat, Mohammad Rastegari, Munish Bansal, Nandhini Santhanam,  
631 Natascha Parks, Natasha White, Navyata Bawa, Nayan Singhal, Nick Egebo, Nicolas Usunier,  
632 Nikhil Mehta, Nikolay Pavlovich Laptev, Ning Dong, Norman Cheng, Oleg Chernoguz, Olivia  
633 Hart, Omkar Salpekar, Ozlem Kalinli, Parkin Kent, Parth Parekh, Paul Saab, Pavan Balaji, Pedro  
634 Rittner, Philip Bontrager, Pierre Roux, Piotr Dollar, Polina Zvyagina, Prashant Ratanchandani,  
635 Pritish Yuvraj, Qian Liang, Rachad Alao, Rachel Rodriguez, Rafi Ayub, Raghotham Murthy,  
636 Raghu Nayani, Rahul Mitra, Rangrabhu Parthasarathy, Raymond Li, Rebekkah Hogan, Robin  
637 Battey, Rocky Wang, Russ Howes, Ruty Rinott, Sachin Mehta, Sachin Siby, Sai Jayesh Bondu,  
638 Samyak Datta, Sara Chugh, Sara Hunt, Sargun Dhillon, Sasha Sidorov, Satadru Pan, Saurabh  
639 Mahajan, Saurabh Verma, Seiji Yamamoto, Sharadh Ramaswamy, Shaun Lindsay, Shaun Lindsay,  
640 Sheng Feng, Shenghao Lin, Shengxin Cindy Zha, Shishir Patil, Shiva Shankar, Shuqiang Zhang,  
641 Shuqiang Zhang, Sinong Wang, Sneha Agarwal, Soji Sajuyigbe, Soumith Chintala, Stephanie  
642 Max, Stephen Chen, Steve Kehoe, Steve Satterfield, Sudarshan Govindaprasad, Sumit Gupta,  
643 Summer Deng, Sungmin Cho, Sunny Virk, Suraj Subramanian, Sy Choudhury, Sydney Goldman,  
644 Tal Remez, Tamar Glaser, Tamara Best, Thilo Koehler, Thomas Robinson, Tianhe Li, Tianjun  
645 Zhang, Tim Matthews, Timothy Chou, Tzook Shaked, Varun Vontimitta, Victoria Ajayi, Victoria  
646 Montanez, Vijai Mohan, Vinay Satish Kumar, Vishal Mangla, Vlad Ionescu, Vlad Poenaru,  
647 Vlad Tiberiu Mihailescu, Vladimir Ivanov, Wei Li, Wenchen Wang, Wenwen Jiang, Wes Bouaziz,  
648 Will Constable, Xiaocheng Tang, Xiaojuan Wu, Xiaolan Wang, Xilun Wu, Xinbo Gao, Yaniv  
649 Kleinman, Yanjun Chen, Ye Hu, Ye Jia, Ye Qi, Yenda Li, Yilin Zhang, Ying Zhang, Yossi Adi,  
650 Youngjin Nam, Yu, Wang, Yu Zhao, Yuchen Hao, Yundi Qian, Yunlu Li, Yuzi He, Zach Rait,  
651 Zachary DeVito, Zef Rosnbrick, Zhaoduo Wen, Zhenyu Yang, Zhiwei Zhao, and Zhiyu Ma. The  
652 llama 3 herd of models, 2024. URL <https://arxiv.org/abs/2407.21783>.

- 648 Zhaoyi Guan, Hongyi Huang, Yihan Su, Haoxiang Huang, Ngai Wong, and Huazhong Yu. Aptq:  
649 Attention-aware post-training mixed-precision quantization for large language models. *arXiv*  
650 *preprint arXiv:2402.14866*, 2024.
- 651 Han Guo, Philip Greengard, Eric Xing, and Yoon Kim. Lq-lora: Low-rank plus quantized matrix  
652 decomposition for efficient language model finetuning. *ICLR 2024*, 2023.
- 653 Han Guo, Philip Greengard, Eric Xing, and Yoon Kim. LQ-loRA: Low-rank plus quantized matrix  
654 decomposition for efficient language model finetuning. In *The Twelfth International Conference*  
655 *on Learning Representations*, 2024. URL <https://openreview.net/forum?id=xw29Vv0MmU>.
- 656 Suyog Gupta, Ankur Agrawal, Kailash Gopalakrishnan, and Pritish Narayanan. Deep learning with  
657 limited numerical precision. In *International conference on machine learning*, pp. 1737–1746.  
658 PMLR, 2015.
- 659 Dan Hendrycks, Collin Burns, Steven Basart, Andy Zou, Mantas Mazeika, Dawn Song, and Jacob  
660 Steinhardt. Measuring massive multitask language understanding. In *International Conference on*  
661 *Learning Representations*, 2021. URL <https://openreview.net/forum?id=d7KBjmI3GmQ>.
- 662 Edward J. Hu, Yelong Shen, Phillip Wallis, Zeyuan Allen-Zhu, Yuanzhi Li, Shean Wang, Lu Wang,  
663 and Weizhu Chen. Lora: Low-rank adaptation of large language models. In *Proceedings of ICLR*,  
664 2022.
- 665 Wei Huang, Haotong Qin, Yangdong Liu, Yawei Li, Qinshuo Liu, Xianglong Liu, Luca Benini,  
666 Michele Magno, Shiming Zhang, and XIAOJUAN QI. Slim-llm: Saliency-driven mixed-precision  
667 quantization for large language models. In *Forty-second International Conference on Machine*  
668 *Learning*.
- 669 Wei Huang, Haotong Qin, Yangdong Liu, Yawei Li, Qinshuo Liu, Xianglong Liu, Luca Benini,  
670 Michele Magno, Shiming Zhang, and Xiaojuan Qi. Slim-llm: Saliency-driven mixed-precision  
671 quantization for large language models, 2025. URL <https://arxiv.org/abs/2405.14917>.
- 672 Sehoon Kim, Connor R. C. Hooper, Amir Gholami, Zhen Dong, Xiuyu Li, Sheng Shen, and  
673 Kurt Keutzer. Squeezellm: Dense-and-sparse quantization. In *Proceedings of the Forty-first*  
674 *International Conference on Machine Learning (ICML)*, 2023.
- 675 Geonho Lee, Janghwan Lee, Sukjin Hong, Minsoo Kim, Euijai Ahn, Du-Seong Chang, and Jungwook  
676 Choi. Rilq: Rank-insensitive lora-based quantization error compensation for boosting 2-bit large  
677 language model accuracy. In *Proceedings of the AAAI Conference on Artificial Intelligence*,  
678 volume 39, pp. 18091–18100, 2025.
- 679 Yixiao Li, Yifan Yu, Chen Liang, Pengcheng He, Nikos Karampatziakis, Weizhu Chen, and Tuo  
680 Zhao. Loftq: Lora-fine-tuning-aware quantization for large language models, 2023. URL <https://arxiv.org/abs/2310.08659>.
- 681 Baohao Liao, Christian Herold, Shahram Khadivi, and Christof Monz. Apiq: Finetuning of 2-bit  
682 quantized large language model. In *Proceedings of the 2024 Conference on Empirical Methods in*  
683 *Natural Language Processing*, pp. 20996–21020, 2024.
- 684 Ji Lin, Jie Tang, Haotao Tang, Shuxin Yang, Xiaoxia Dang, and Song Han. Awq: Activation-aware  
685 weight quantization for llm compression and acceleration. *arXiv preprint arXiv:2306.00978*, 2023.
- 686 Hanxiao Liu, Karen Simonyan, and Yiming Yang. Darts: Differentiable architecture search. In  
687 *International Conference on Learning Representations*.
- 688 Shih-Yang Liu, Chien-Yi Wang, Hongxu Yin, Pavlo Molchanov, Yu-Chiang Frank Wang, Kwang-  
689 Ting Cheng, and Min-Hung Chen. Dora: Weight-decomposed low-rank adaptation. In *Forty-first*  
690 *International Conference on Machine Learning*, 2024a.
- 691 Zechun Liu, Changsheng Zhao, Igor Fedorov, Bilge Soran, Dhruv Choudhary, Raghuraman Krish-  
692 namoorthi, Vikas Chandra, Yuandong Tian, and Tijmen Blankevoort. Spiquant: Llm quantization  
693 with learned rotations. In *The Thirteenth International Conference on Learning Representations*,  
694 2024b.

- 702 Spyros Makridakis, Fotios Petropoulos, and Yanfei Kang. Large language models: Their success and  
703 impact. *Forecasting*, 5(3):536–549, 2023.  
704
- 705 Todor Mihaylov, Peter Clark, Tushar Khot, and Ashish Sabharwal. Can a suit of armor conduct  
706 electricity? a new dataset for open book question answering. In *Proceedings of the 2018 Conference*  
707 *on Empirical Methods in Natural Language Processing*, pp. 2381–2391, 2018.
- 708 Qwen, :, An Yang, Baosong Yang, Beichen Zhang, Binyuan Hui, Bo Zheng, Bowen Yu, Chengyuan  
709 Li, Dayiheng Liu, Fei Huang, Haoran Wei, Huan Lin, Jian Yang, Jianhong Tu, Jianwei Zhang,  
710 Jianxin Yang, Jiayi Yang, Jingren Zhou, Junyang Lin, Kai Dang, Keming Lu, Keqin Bao, Kexin  
711 Yang, Le Yu, Mei Li, Mingfeng Xue, Pei Zhang, Qin Zhu, Rui Men, Runji Lin, Tianhao Li, Tianyi  
712 Tang, Tingyu Xia, Xingzhang Ren, Xuancheng Ren, Yang Fan, Yang Su, Yichang Zhang, Yu Wan,  
713 Yuqiong Liu, Zeyu Cui, Zhenru Zhang, and Zihan Qiu. Qwen2.5 technical report, 2025. URL  
714 <https://arxiv.org/abs/2412.15115>.
- 715 Mohaimenul Azam Khan Raiaan, Md Saddam Hossain Mukta, Kaniz Fatema, Nur Mohammad  
716 Fahad, Sadman Sakib, Most Marufatul Jannat Mim, Jubaer Ahmad, Mohammed Eunus Ali, and  
717 Sami Azam. A review on large language models: Architectures, applications, taxonomies, open  
718 issues and challenges. *IEEE Access*, 2024.  
719
- 720 Keisuke Sakaguchi, Ronan Le Bras, Chandra Bhagavatula, and Yejin Choi. Winogrande: An  
721 adversarial winograd schema challenge at scale. *Communications of the ACM*, 64(9):99–106,  
722 2021.
- 723 Rohan Taori, Ishaan Gulrajani, Tianyi Zhang, Yann Dubois, Xuechen Li, Carlos Guestrin, Percy  
724 Liang, and Tatsunori B. Hashimoto. Stanford alpaca: An instruction-following llama model.  
725 *Stanford CRFM*, 2023. URL [https://github.com/tatsu-lab/stanford\\_alpaca](https://github.com/tatsu-lab/stanford_alpaca).
- 726 Hugo Touvron, Louis Martin, Kevin Stone, Peter Albert, Amjad Almahairi, Yasmine Babaei, Nikolay  
727 Bashlykov, Soumya Batra, Prajjwal Bhargava, and et al. Bhosale, Shruti. Llama 2: Open foundation  
728 and fine-tuned chat models. *arXiv preprint arXiv:2307.09288*, 2023.  
729
- 730 Zhongwei Wan, Xin Wang, Che Liu, Samiul Alam, Yu Zheng, Jiachen Liu, Zhongnan Qu, Shen Yan,  
731 Yi Zhu, Quanlu Zhang, et al. Efficient large language models: A survey. *Transactions on Machine*  
732 *Learning Research*, 2023.
- 733 Hanrui Wang, Zhanghao Wu, Zhijian Liu, Han Cai, Ligeng Zhu, Chuang Gan, and Song Han. Hat:  
734 Hardware-aware transformers for efficient natural language processing. In *Proceedings of the 58th*  
735 *Annual Meeting of the Association for Computational Linguistics*, pp. 7675–7688, 2020.  
736
- 737 Xinyuan Wang, Yanchi Liu, Wei Cheng, Xujiang Zhao, Zhengzhang Chen, Wenchao Yu, Yanjie  
738 Fu, and Haifeng Chen. Mixllm: Dynamic routing in mixed large language models, 2025. URL  
739 <https://arxiv.org/abs/2502.18482>.
- 740 Guangxuan Xiao, Ji Lin, Mickael Seznec, Hao Wu, Julien Demouth, and Song Han. Smoothquant:  
741 Accurate and efficient post-training quantization for large language models. *arXiv:2211.10438*,  
742 2022.
- 743 Guangxuan Xiao, Ji Lin, Mickael Seznec, Hao Wu, Julien Demouth, and Song Han. Smoothquant:  
744 Accurate and efficient post-training quantization for large language models. In *International*  
745 *conference on machine learning*, pp. 38087–38099. PMLR, 2023.  
746
- 747 Zhewei Yao, Reza Yazdani Aminabadi, Ming Zhang, Xiang Wu, Cong Li, and Yuxiong He. Zeroquant:  
748 Efficient and affordable post-training quantization for large-scale transformers. In *Advances in*  
749 *Neural Information Processing Systems*, volume 35, pp. 27168–27183, 2022.
- 750 Rowan Zellers, Ari Holtzman, Yonatan Bisk, Ali Farhadi, and Yejin Choi. Hellaswag: Can a machine  
751 really finish your sentence? In *Proceedings of the 57th Annual Meeting of the Association for*  
752 *Computational Linguistics*, pp. 4791–4800, 2019.  
753
- 754 Qingru Zhang, Minshuo Chen, Alexander Bukharin, Pengcheng He, Yu Cheng, Weizhu Chen, and Tuo  
755 Zhao. Adaptive budget allocation for parameter-efficient fine-tuning. In *International Conference*  
*on Learning Representations*. Openreview, 2023a.

756 Qingru Zhang, Minshuo Chen, Alexander Bukharin, Nikos Karampatziakis, Pengcheng He, Yu Cheng,  
757 Weizhu Chen, and Tuo Zhao. Adalora: Adaptive budget allocation for parameter-efficient fine-  
758 tuning. *arXiv preprint arXiv:2303.10512*, 2023b.

759  
760 Changhai Zhou, Shijie Han, Shiyang Zhang, Shichao Weng, Zekai Liu, and Cheng Jin. Rankadap-  
761 tor: Hierarchical dynamic low-rank adaptation for structural pruned llms. *arXiv preprint*  
762 *arXiv:2406.15734*, 2024.

763 Changhai Zhou, Shijie Han, Lining Yang, Yuhua Zhou, Xu Cheng, Yibin Wang, and Hongguang Li.  
764 RankAdaptor: Hierarchical rank allocation for efficient fine-tuning pruned LLMs via performance  
765 model. In Luis Chiruzzo, Alan Ritter, and Lu Wang (eds.), *Findings of the Association for*  
766 *Computational Linguistics: NAACL 2025*, pp. 5781–5795, Albuquerque, New Mexico, April 2025.  
767 Association for Computational Linguistics. ISBN 979-8-89176-195-7. doi: 10.18653/v1/2025.  
768 findings-naacl.321. URL <https://aclanthology.org/2025.findings-naacl.321/>.

769  
770  
771  
772  
773  
774  
775  
776  
777  
778  
779  
780  
781  
782  
783  
784  
785  
786  
787  
788  
789  
790  
791  
792  
793  
794  
795  
796  
797  
798  
799  
800  
801  
802  
803  
804  
805  
806  
807  
808  
809

810  
811  
812  
813  
814  
815  
816  
817  
818  
819  
820  
821  
822  
823  
824  
825  
826  
827  
828  
829  
830  
831  
832  
833  
834  
835  
836  
837  
838  
839  
840  
841  
842  
843  
844  
845  
846  
847  
848  
849  
850  
851  
852  
853  
854  
855  
856  
857  
858  
859  
860  
861  
862  
863

## Table of Contents

---

<b>A Extended Related Work</b>	<b>17</b>
<b>B Use of LLMs</b>	<b>17</b>
<b>C On the Suboptimality of Continuous Proxies for Discrete Quantization</b>	<b>17</b>
C.1 Problem Formulation: Quantization as Projection . . . . .	18
C.2 Analysis of Iterative Low-Rank Refinement . . . . .	18
C.3 Formal Argument for Suboptimality . . . . .	18
C.4 The Discontinuous Optimization Landscape . . . . .	19
<b>D Quantization</b>	<b>19</b>
<b>E QR-Adaptor Search Process Details</b>	<b>20</b>
E.1 Search Hyperparameters and Configuration . . . . .	20
E.2 Task-Informed Initialization Algorithm . . . . .	20
<b>F Pseudo code of the specific algorithm in the QR-Adaptor framework</b>	<b>21</b>
<b>G More Results</b>	<b>21</b>
G.1 Experiment Scope Expansion: Llama 2 Series . . . . .	21
G.2 Visualization Results for the MMLU Task . . . . .	22
G.3 Effectiveness on Larger Datasets with Higher Ranks . . . . .	23
G.4 Fairer Comparison: Matching Bit-width Configurations . . . . .	24
G.5 Impact of Longer Fine-tuning Epochs on Unfixed Parameters . . . . .	25
G.6 Impact of 2-Bit Quantization and LoftQ Iterations . . . . .	26
<b>H Version of LLMs</b>	<b>27</b>
<b>I More Implementation Details</b>	<b>27</b>
<b>J More Ablation</b>	<b>27</b>
J.1 Gradient Norms vs. Relative Entropy . . . . .	27
J.2 Sensitivity to Iteration Counts and Population Size . . . . .	28
<b>K Visualization of Optimization Stages</b>	<b>28</b>
<b>L Limitation</b>	<b>29</b>

---



## 864 A EXTENDED RELATED WORK

865  
866 **LLM Quantization.** The field of LLM quantization has witnessed substantial progress, driven by the  
867 need for efficient model deployment. Recent research has introduced several innovative approaches.  
868 Frantar et al. (2023) developed GPTQ, achieving 4-bit precision with layer-wise quantization. Lin  
869 et al. (2023) proposed AWQ, improving accuracy for heavily quantized models. Xiao et al. (2023)  
870 introduced SmoothQuant, addressing quantization of both weights and activations. Yao et al. (2022)  
871 introduced ZeroQuant, preserving zero-shot capabilities at low bit widths. Dettmers et al. (2022)  
872 presented LLM.int8(), enabling 8-bit quantization on consumer hardware. Kim et al. (2023) combined  
873 quantization with pruning and knowledge distillation in SqueezeLLM. Mixed-precision quantization  
874 has further advanced the field: APTQ Guan et al. (2024) balances compression and performance,  
875 MixLLM Wang et al. (2025) employs dynamic strategies, and Slim-LLM Huang et al. provides  
876 another mixed-precision solution. These works highlight the importance of per-layer allocation but  
877 focus exclusively on quantization.

878 **Parameter Efficient Fine-Tuning.** PEFT techniques enhance LLMs without raising inference costs.  
879 QLoRA Dettmers et al. (2023) combines 4-bit quantization with low-rank adapters, while LoftQ Li  
880 et al. (2023) alternates between quantization and low-rank steps. CoLoRA Berman & Peherstorfer  
881 (2024) accelerates predictions under new parameters. AdaLoRA Zhang et al. (2023a) adaptively  
882 allocates update budgets; LQ-LoRA Guo et al. (2023) merges decomposition and quantization;  
883 RankAdaptor Zhou et al. (2024) enables hierarchical dynamic adaptation; DoRA Liu et al. (2024a)  
884 decomposes weights into magnitude and direction. While these approaches account for heterogeneous  
885 adaptation needs, they largely remain orthogonal to quantization.

886 **Joint Quantization and Low-Rank Adaptation.** Some works integrate quantization and adaptation.  
887 LoftQ Li et al. (2023) alternates quantization with low-rank approximation using SVD initialization,  
888 but iterative error fitting may degrade performance. LQ-LoRA Guo et al. (2023) combines low-rank  
889 decomposition with quantization, allocating bit-widths based on error budgets, though rank is treated  
890 separately. These methods are important steps but optimize quantization and adaptation independently  
891 or via proxy metrics, leaving open the challenge of jointly allocating memory between precision and  
892 rank per layer.

893 **Neural Architecture Search and Optimization.** Joint optimization of quantization and adaptation  
894 parameters connects to neural architecture search. DARTS Liu et al. introduced differentiable  
895 architecture search, and HAT Wang et al. (2020) proposed hardware-aware transformers. However,  
896 they primarily explore architecture design, not the discrete per-layer precision–rank allocation  
897 problem. Our discrete optimization requires specialized search strategies; genetic algorithms and  
898 Bayesian optimization offer promising directions, motivating our three-stage approach combining  
899 task-informed initialization, global exploration, and local refinement.

## 900 B USE OF LLMs

901  
902 In preparing this paper, LLMs were employed solely for language refinement purposes, such as  
903 improving grammar, clarity, and style of expression. All research questions, conceptual frameworks,  
904 theoretical arguments, methodological designs, data analyses, and conclusions presented in this work  
905 were independently conceived and executed by the author. The LLMs did not generate, alter, or  
906 influence the underlying ideas, interpretations, or findings. Their use was limited to assisting in  
907 polishing the readability and fluency of the manuscript while preserving the originality and integrity  
908 of the scholarly contributions.  
909

## 910 C ON THE SUBOPTIMALITY OF CONTINUOUS PROXIES FOR DISCRETE 911 QUANTIZATION

912  
913 This appendix provides a formal analysis of why iterative fine-tuning methods that rely on continuous,  
914 low-rank updates to correct quantization error can be suboptimal. These methods, such as LoftQ,  
915 operate by minimizing a continuous objective (e.g., Frobenius norm) but ultimately must project the  
916 result back into a discrete space for inference. We demonstrate that this two-stage process does not  
917

918 guarantee finding the optimal discrete representation, thereby motivating our gradient-free, direct  
 919 search approach in the discrete configuration space.

### 921 C.1 PROBLEM FORMULATION: QUANTIZATION AS PROJECTION

922 We begin by defining the quantization process as a projection onto a discrete lattice.

923 **Definition C.1** (Quantization Lattice and Operator). For a given bit-width, the set of representable  
 924 scalar values forms a uniform grid with step size  $\Delta$ . For a weight matrix  $\mathbf{W} \in \mathbb{R}^{d \times k}$ , the correspond-  
 925 ing quantization lattice  $\Lambda$  is the set of all matrices whose elements belong to this grid:  
 926

$$927 \Lambda = \{\mathbf{M} \in \mathbb{R}^{d \times k} \mid M_{ij} = n_{ij}\Delta \text{ for some } n_{ij} \in \mathbb{Z}\}. \quad (8)$$

928 The standard quantization operator,  $\text{Quantize}(\cdot)$ , performs an element-wise rounding operation that  
 929 maps a continuous matrix to the nearest point in the lattice  $\Lambda$ . This operator is equivalent to a  
 930 projection onto  $\Lambda$ :  
 931

$$932 \mathbf{W}_q = \text{Quantize}(\mathbf{W}) = \mathcal{P}_\Lambda(\mathbf{W}) = \arg \min_{\mathbf{M} \in \Lambda} \|\mathbf{W} - \mathbf{M}\|_F. \quad (9)$$

933 The core objective of quantization-aware fine-tuning is to find a matrix  $\mathbf{W}'_q \in \Lambda$  that not only  
 934 minimizes the memory footprint but also maximizes downstream task performance. Ideally, this  
 935  $\mathbf{W}'_q$  should be a good approximation of the optimal full-precision weights  $\mathbf{W}^*$  for a given task. For  
 936 simplicity in this analysis, we consider the goal to be finding the closest lattice point to a target  
 937 full-precision matrix  $\mathbf{W}$ , i.e., finding  $\mathcal{P}_\Lambda(\mathbf{W})$ .  
 938

### 941 C.2 ANALYSIS OF ITERATIVE LOW-RANK REFINEMENT

942 Methods like LoftQ attempt to improve upon the initial quantization  $\mathbf{W}_q = \mathcal{P}_\Lambda(\mathbf{W})$  by adding a  
 943 continuous low-rank correction. The process can be described as follows:  
 944

- 945 1. **Initial Quantization:** Start with the baseline quantized matrix  $\mathbf{W}_q = \mathcal{P}_\Lambda(\mathbf{W})$ .
- 946 2. **Continuous Error Correction:** Define the quantization error as  $\mathbf{E} = \mathbf{W} - \mathbf{W}_q$ . Find a  
 947 low-rank approximation  $\mathbf{AB}^*$  to this error by minimizing a continuous objective:  
 948

$$949 \mathbf{AB}^* = \arg \min_{\text{rank}(\mathbf{AB}) \leq r} \|\mathbf{E} - \mathbf{AB}\|_F = \arg \min_{\text{rank}(\mathbf{AB}) \leq r} \|\mathbf{W} - (\mathbf{W}_q + \mathbf{AB})\|_F. \quad (10)$$

950 The solution is typically found via Singular Value Decomposition (SVD) of the error matrix  
 951  $\mathbf{E}$ .

- 952 3. **Final Discretization:** The resulting matrix,  $\mathbf{W}_{\text{updated}} = \mathbf{W}_q + \mathbf{AB}^*$ , is continuous and not  
 953 in  $\Lambda$ . For inference, it must be re-quantized:  
 954

$$955 \mathbf{W}'_q = \mathcal{P}_\Lambda(\mathbf{W}_{\text{updated}}) = \mathcal{P}_\Lambda(\mathbf{W}_q + \mathbf{AB}^*). \quad (11)$$

956 The critical question is whether this process reliably yields the best possible discrete approximation.  
 957 That is, does  $\mathbf{W}'_q$  equal the true optimal solution,  $\mathcal{P}_\Lambda(\mathbf{W})$ ?  
 958

### 961 C.3 FORMAL ARGUMENT FOR SUBOPTIMALITY

962 The procedure described above is suboptimal because the continuous optimization in Step 2 is  
 963 disconnected from the final discrete projection in Step 3.  
 964

965 **Proposition C.2.** *Let  $\mathbf{W}_{\text{opt}} = \mathcal{P}_\Lambda(\mathbf{W})$  be the optimal discrete approximation of  $\mathbf{W}$ . Let  $\mathbf{W}'_q =$   
 966  $\mathcal{P}_\Lambda(\mathbf{W}_q + \mathbf{AB}^*)$  be the matrix obtained from the iterative refinement process. It is not guaranteed  
 967 that  $\mathbf{W}'_q = \mathbf{W}_{\text{opt}}$ . In high-dimensional spaces, they are often different.  
 968*

969 *Justification.* The projection operator  $\mathcal{P}_\Lambda$  partitions the continuous space  $\mathbb{R}^{d \times k}$  into a set of disjoint  
 970 Voronoi cells, one for each lattice point  $\mathbf{M} \in \Lambda$ . A point  $\mathbf{Y}$  is projected to  $\mathbf{M}$  if and only if it lies  
 971 within the Voronoi cell of  $\mathbf{M}$ , denoted  $V(\mathbf{M})$ .

1. By definition, the optimal discrete solution is  $\mathbf{W}_{\text{opt}} = \mathcal{P}_\Lambda(\mathbf{W})$ , which means the original matrix  $\mathbf{W}$  lies inside the Voronoi cell  $V(\mathbf{W}_{\text{opt}})$ . In our simplified case where  $\mathbf{W}_q$  is the initial rounding,  $\mathbf{W}_{\text{opt}} = \mathbf{W}_q$ , so  $\mathbf{W} \in V(\mathbf{W}_q)$ .
2. The iterative method computes an updated continuous matrix  $\mathbf{W}_{\text{updated}} = \mathbf{W}_q + \mathbf{A}\mathbf{B}^*$ . Substituting the definitions, we have:

$$\mathbf{W}_{\text{updated}} = \mathbf{W} - \mathbf{E} + \mathbf{A}\mathbf{B}^* = \mathbf{W} - (\mathbf{E} - \mathbf{A}\mathbf{B}^*). \tag{12}$$

Here,  $\mathbf{E} - \mathbf{A}\mathbf{B}^*$  is the residual error from the low-rank approximation of the quantization error  $\mathbf{E}$ .

3. The final quantized matrix is  $\mathbf{W}'_q = \mathcal{P}_\Lambda(\mathbf{W}_{\text{updated}})$ . This means  $\mathbf{W}_{\text{updated}}$  must lie in the Voronoi cell  $V(\mathbf{W}'_q)$ .
4. For the method to be optimal (i.e.,  $\mathbf{W}'_q = \mathbf{W}_{\text{opt}}$ ), the updated point  $\mathbf{W}_{\text{updated}}$  must lie in the same Voronoi cell as the original point  $\mathbf{W}$ . However, the term  $\delta = \mathbf{E} - \mathbf{A}\mathbf{B}^*$  acts as a perturbation on  $\mathbf{W}$ . The quantization error  $\mathbf{E}$  is typically a dense, noisy, high-rank matrix. Its low-rank approximation error  $\delta$  is therefore also a high-rank matrix.

Adding this high-rank perturbation  $\delta$  to  $\mathbf{W}$  can easily push the vector across a Voronoi boundary into an adjacent cell. When  $\mathbf{W} - \delta$  falls into a different cell  $V(\mathbf{M})$  where  $\mathbf{M} \neq \mathbf{W}_{\text{opt}}$ , the final projection becomes suboptimal:  $\mathcal{P}_\Lambda(\mathbf{W}_{\text{updated}}) = \mathbf{M} \neq \mathbf{W}_{\text{opt}}$ . This occurs generically in high dimensions, as even a small perturbation has many dimensions in which it can push the vector across a boundary. The assumption that minimizing the continuous error  $\|\mathbf{W} - \mathbf{W}_{\text{updated}}\|_F$  will keep  $\mathbf{W}_{\text{updated}}$  in the correct Voronoi cell is unfounded. ■

#### C.4 THE DISCONTINUOUS OPTIMIZATION LANDSCAPE

The suboptimality issue is further compounded by the nature of the true underlying objective function. If we consider the downstream loss  $\mathcal{L}$ , the function we implicitly want to optimize with respect to  $\mathbf{A}$  and  $\mathbf{B}$  is:

$$f(\mathbf{A}, \mathbf{B}) = \mathcal{L}(\mathcal{P}_\Lambda(\mathbf{W}_q + \mathbf{A}\mathbf{B})). \tag{13}$$

Due to the discrete nature of the projection  $\mathcal{P}_\Lambda$ , this function is piecewise constant. Small, continuous changes to  $\mathbf{A}$  and  $\mathbf{B}$  will not change the output of  $\mathcal{P}_\Lambda(\mathbf{W}_q + \mathbf{A}\mathbf{B})$  as long as the matrix remains within its current Voronoi cell. The function value only changes when  $\mathbf{W}_q + \mathbf{A}\mathbf{B}$  crosses a boundary into a new cell.

This has a critical implication for optimization:

- **Vanishing Gradients:** The gradient  $\nabla_{\mathbf{A}, \mathbf{B}} f(\mathbf{A}, \mathbf{B})$  is zero almost everywhere (within the interior of each Voronoi cell).
- **Optimization Stagnation:** Gradient-based methods are ineffective in such a landscape. They receive no signal to guide the updates of  $\mathbf{A}$  and  $\mathbf{B}$  and will stagnate unless an update is large enough to jump to a new discrete state.

**Conclusion.** The analysis reveals two fundamental flaws in using continuous proxies for discrete optimization. First, minimizing a continuous error metric does not guarantee finding the optimal discrete solution after re-quantization. Second, the true objective landscape is piecewise constant, rendering standard gradient-based optimization ineffective. These limitations strongly motivate a shift away from continuous proxies and towards methods that directly search the discrete space of configurations. Our QR-Adaptor framework, which uses a gradient-free, multi-objective search to evaluate discrete (bit-width, rank) configurations based on their actual downstream performance, is a principled response to these challenges.

## D QUANTIZATION

We first apply NF-quantization with bit size  $b_0$  and bucket size  $B_0$  to obtain the quantized matrix  $\widehat{A}_i$  and the absmax values for each block  $s = [s_1, \dots, s_{\frac{\text{sizeof}(A_i)}{B_0}}]$ . These absmax values are further

quantized to  $b_1$  bits via uniform integer quantization with bucket size  $B_1$  to obtain the quantized vector  $\hat{s}$ , along with the absmax values for  $s$ , i.e.,  $v = [v_1, \dots, v_{\frac{\text{sizeof}(A_i)}{B_0 B_1}}]$ . Finally, we cast  $v$  to  $b_2$  bits to obtain  $\hat{v}$ .

This quantization scheme requires storing  $\widehat{A}_i, \widehat{s}, \widehat{v}$  to represent  $A_i$ . We can thus quantify the memory cost (number of bits) for storing  $A_i$  given a configuration  $c_i = (b_0, b_1, b_2, B_0, B_1)$  as:

$$\text{memory\_cost}(A_i, c_i) = \text{sizeof}(A_i) \cdot \left( b_0 + \frac{b_1}{B_0} + \frac{b_2}{B_0 \cdot B_1} \right) \quad (14)$$

The original NF-4 double quantization is a special case with  $q_{\text{NF4}} = (4, 8, \text{fp32}, 64, 256)$  and  $\text{memory\_cost}(A_i, q_{\text{NF4}}) = 4.127 \cdot \text{sizeof}(A_i)$ , i.e., NF-4 requires on average 4.127 bits per parameter.

## E QR-ADAPTOR SEARCH PROCESS DETAILS

This appendix provides supplementary details regarding the QR-Adaptor search methodology and its associated computational costs, addressing reproducibility and practical implementation concerns.

### E.1 SEARCH HYPERPARAMETERS AND CONFIGURATION

To ensure the reproducibility of our results, we list the specific hyperparameters and configurations used for the QR-Adaptor search process in Table 6. These settings were kept consistent across all main experiments unless otherwise noted.

**Table 6:** Hyperparameters for the QR-Adaptor search process.

Parameter	Stage	Value / Description
<b>General Search Configuration</b>		
Bit-width Search Space ( $\mathcal{Q}$ )	All	{2, 4, 8}
LoRA Rank Search Space ( $\mathcal{R}$ )	All	{0, 2, 4, 6, 8, ..., 64}
Calibration Dataset	All	A random subset of 1024 samples from the C4 dataset.
Fine-tuning Epochs (per evaluation)	All	1 epoch on the calibration dataset.
<b>Stage 1: Task-Informed Initialization</b>		
Importance Score Metric ( $I(l)$ )	Initialization	Gradient-based saliency score (magnitude of Fisher Information).
Initial Population Size ( $N_{\text{pop}}$ )	Initialization	1
<b>Stage 2: Global Exploration (PRGA)</b>		
Algorithm	PRGA	NSGA-II (Non-dominated Sorting Genetic Algorithm II)
Number of Generations	PRGA	5
Population Size	PRGA	20
Selection Mechanism	PRGA	Tournament selection based on non-dominated rank and crowding distance.
Crossover Operator	PRGA	Uniform Crossover with a probability of 0.9.
Mutation Operator	PRGA	Per-layer random mutation: for each layer, with probability 0.1, re-sample its bit-width and rank from $\mathcal{Q}$ and $\mathcal{R}$ .
<b>Stage 3: Local Refinement (Bayesian Optimization)</b>		
Surrogate Model	BO	Gaussian Process (GP)
GP Kernel	BO	Matérn 5/2 kernel with Automatic Relevance Determination (ARD).
Acquisition Function	BO	Expected Improvement (EI).
Number of Iterations	BO	5 iterations per configuration refined from the Pareto front.

### E.2 TASK-INFORMED INITIALIZATION ALGORITHM

As mentioned in Section 3.2.1, the initialization process uses layer importance scores to generate a high-quality initial configuration. Algorithm 3 provides a concrete step-by-step description of this procedure. The core idea is to map higher importance scores to a higher probability of allocating more resources (i.e., higher bit-widths and ranks). **This single seed configuration  $C_0$  is evaluated by fine-tuning for one epoch on the calibration dataset to measure its initial performance**, forming the starting point for the global search. The subsequent PRGA stage will generate a full population of size 20 through mutations and crossover operations based on this seed.

**Algorithm 3** Task-Informed Initialization Process

---

```

1080 1: Input: Layer importance scores  $\{I(l)\}_{l=1}^L$ , Bit-width space  $\mathcal{Q}$ , Rank space  $\mathcal{R}$ .
1081 2: Output: Seed configuration  $C_0$ .
1082 3:  $\triangleright$  Step 1: Normalize importance scores to create a sampling distribution
1083 4: Normalize scores:  $p_l \leftarrow I(l) / \sum_{j=1}^L I(j)$  for  $l = 1, \dots, L$ .
1084 5:  $\triangleright$  Step 2: Generate the seed configuration  $C_0$  based on importance
1085 6: Initialize  $C_0 = [(\text{bit}_1, \text{rank}_1), \dots, (\text{bit}_L, \text{rank}_L)]$ .
1086 7: for  $l = 1$  to  $L$  do
1087 8:   // Map normalized importance  $p_l$  to the search spaces.
1088 9:   // The higher the importance, the higher the index in the sorted space.
1089 10:   Sort  $\mathcal{Q}$  and  $\mathcal{R}$  in ascending order.
1090 11:   Bit index  $idx_b \leftarrow \lfloor p_l \cdot (|\mathcal{Q}| - 1) \rfloor$ . Clamp to  $[0, |\mathcal{Q}| - 1]$ .
1091 12:   Rank index  $idx_r \leftarrow \lfloor p_l \cdot (|\mathcal{R}| - 1) \rfloor$ . Clamp to  $[0, |\mathcal{R}| - 1]$ .
1092 13:    $\text{bit}_l \leftarrow \mathcal{Q}[idx_b]$ ;  $\text{rank}_l \leftarrow \mathcal{R}[idx_r]$ .
1093 14: end for
1094 15:  $\triangleright$  Step 3: (Optional) Apply budget constraints if a target budget is predefined
1095 16: return  $C_0$ .

```

---

## F PSEUDO CODE OF THE SPECIFIC ALGORITHM IN THE QR-ADAPTOR FRAMEWORK

Due to page limitations, we present the pseudocode of the algorithm.

**Algorithm 4** Pareto Rank Calculation

---

```

1105 1: Input: Population  $P$  with  $n$  individuals
1106 2: Calculate the number of dominated individuals  $n_p$  and the set of solutions dominated
1107 3:  $S_p$  for each individual  $p$ 
1108 4: Place individuals with  $n_p = 0$  into set  $F_1$ 
1109 5: for each individual  $i$  in  $F_1$  do
1110 6:   for each individual  $j \in S_i$  do
1111 7:      $n_j \leftarrow n_j - 1$ 
1112 8:     if  $n_j = 0$  then
1113 9:       Add individual  $j$  to set  $F_2$ 
1114 10:     end if
1115 11:   end for
1116 12: end for
1117 13: Repeat for  $F_2, F_3, \dots$ , until all individuals
1118 14: are ranked
1119 15: Output: Pareto-ranked individuals

```

---

**Algorithm 5** Crowding Distance Calculation

---

```

1120 1: Input: Ranked individuals  $F$  with  $N$  individuals,  $M$  objectives
1121 2: for each individual  $n \in 1 \dots N$  do
1122 3:   Initialize  $d_n \leftarrow 0$ 
1123 4: end for
1124 5: for each objective function  $f_m$  do
1125 6:   Sort individuals based on  $f_m$ 
1126 7:    $f_m^{max}, f_m^{min} \leftarrow \max f_m, \min f_m$ 
1127 8:    $d_1, d_N \leftarrow \infty$ 
1128 9:   for  $n = 2$  to  $N - 1$  do
1129 10:      $d_n \leftarrow d_n + \frac{f_m^{(n+1)} - f_m^{(n-1)}}{f_m^{max} - f_m^{min}}$ 
1130 11:   end for
1131 12: end for
1132 13: Output: Crowding distances  $d_n$  for each
1133 14: individual  $n$ 

```

---

## G MORE RESULTS

Due to page limitations, we present remaining results across various models here.

### G.1 EXPERIMENT SCOPE EXPANSION: LLAMA 2 SERIES

In the original experiments, the focus was primarily on Llama3.1, considering that its updated architecture present new challenges for quantization. Compared to Llama2 series, Llama3.1 is significantly harder to quantize, especially under low-bit configurations, as they incorporate more sophisticated architectural features. Additionally, to comprehensively demonstrate the superiority of **QR-Adaptor**, we have also conducted extensive performance experiments on the Llama2 series models, with the results presented in Table 7 and Table 8.

**Algorithm 6** Simulated Binary Crossover (SBX)

**Require:** Two parent individuals  $P_1$  and  $P_2$ , each with  $L$  real-valued genes

- 1: Initialize offspring  $O_1$  and  $O_2$  as empty
- 2: **for**  $l = 1$  to  $L$  **do**
- 3:     Generate a random number  $u \in [0, 1]$
- 4:     **if**  $u \leq 0.5$  **then**
- 5:          $\beta \leftarrow (2u)^{1/(n+1)}$
- 6:     **else**
- 7:          $\beta \leftarrow \left(\frac{1}{2(1-u)}\right)^{1/(n+1)}$
- 8:     **end if**
- 9:      $y_{1l} \leftarrow 0.5 \cdot ((1 + \beta) \cdot p_{1l} + (1 - \beta) \cdot p_{2l})$
- 10:     $y_{2l} \leftarrow 0.5 \cdot ((1 - \beta) \cdot p_{1l} + (1 + \beta) \cdot p_{2l})$
- 11:    Append  $y_{1l}$  to  $O_1$  and  $y_{2l}$  to  $O_2$
- 12: **end for**
- 13: **Output:**  $O_1$  and  $O_2$

**Algorithm 7** Polynomial Mutation

**Require:** Individual  $P$  with  $L$  real-valued genes, mutation probability  $p_m$

- 1: Initialize mutated individual  $P'$  as a copy of  $P$
- 2: **for**  $l = 1$  to  $L$  **do**
- 3:     Generate a random number  $u \in [0, 1]$
- 4:     **if**  $u < p_m$  **then**
- 5:         Generate a random number  $\delta \in [-1, 1]$
- 6:          $x'_l \leftarrow x_l + (x_{max} - x_{min}) \cdot \delta \cdot (1 - |\delta|)^{n-1}$
- 7:         Replace  $x_l$  with  $x'_l$  in  $P'$
- 8:     **end if**
- 9: **end for**
- 10: **Output:** Mutated individual  $P'$

**Table 7:** Performance comparison of different methods across various bit-width configurations on Llama2-7B. Superscripts on LoftQ bits indicate the number of initialization iterations. QR-Adaptor for optimal bit number and rank value for each layer based on different tasks with its bit number averaged across tasks. Bold figures represent the best performance for a given model and task, while underlined figures indicate the second-best. Accuracy is reported as %.

	Method	Bit	ARC(C)	ARC(E)	BoolQ	HellaS	OBQA	PIQA	WinoG	Average
Rank = 8	LoRA	16	46.93	<u>77.36</u>	<u>78.47</u>	<b>76.93</b>	44.80	79.38	69.38	67.61
	QLoRA	8	<b>48.21</b>	<u>77.36</u>	77.92	76.88	44.80	<u>79.82</u>	68.75	<u>67.70</u>
	QLoRA	4	46.25	76.26	77.43	76.42	<b>46.20</b>	<u>78.67</u>	<u>69.85</u>	67.30
	AdaLoRA	16	46.08	76.77	77.46	75.89	44.20	79.16	69.22	66.97
	AdaLoRA	8	46.08	76.73	77.49	75.93	44.20	79.00	69.06	66.93
	AdaLoRA	4	46.33	75.25	76.39	75.45	44.40	77.91	69.14	66.41
	LoftQ	4 <sup>1</sup>	46.16	77.10	77.43	76.68	44.80	79.33	69.30	67.26
	LoftQ	4 <sup>5</sup>	47.35	76.64	76.33	76.36	45.60	79.05	69.06	67.20
	LQ-LoRA	4	47.18	76.60	76.54	76.24	45.00	78.84	68.90	67.04
	QR-Adaptor	5.45	<u>48.04</u>	<b>77.44</b>	<b>78.96</b>	76.84	<u>46.00</u>	<b>79.86</b>	<b>69.97</b>	<b>68.15</b>
Rank = 16	LoRA	16	46.93	<b>77.57</b>	<u>78.41</u>	76.81	45.00	79.38	69.06	67.59
	QLoRA	8	47.61	<u>77.44</u>	<u>78.41</u>	<b>76.93</b>	45.40	79.05	69.06	67.70
	QLoRA	4	46.67	76.35	77.25	76.40	45.00	78.84	<u>70.01</u>	67.22
	AdaLoRA	16	46.16	76.68	77.58	75.92	44.20	79.11	69.38	67.00
	AdaLoRA	8	46.16	76.68	77.40	75.91	44.40	79.11	69.06	66.96
	AdaLoRA	4	46.33	75.29	76.45	75.44	44.20	77.91	69.46	66.47
	LoftQ	4 <sup>1</sup>	47.10	77.19	77.89	76.61	44.80	<u>79.43</u>	69.69	67.53
	LoftQ	4 <sup>5</sup>	<u>47.95</u>	76.47	76.79	76.25	45.60	<u>78.51</u>	69.61	67.31
	LQ-LoRA	4	47.10	76.39	77.22	76.33	<b>46.40</b>	78.78	<b>70.09</b>	67.47
	QR-Adaptor	5.45	<b>48.04</b>	<u>77.44</u>	<b>78.96</b>	<u>76.84</u>	<u>46.00</u>	<b>79.86</b>	69.97	<b>68.15</b>

Our results show that **QR-Adaptor** consistently demonstrates superior performance across all tasks and outperforms existing methods, such as AdaLoRA and LoftQ, on Llama 2 series. The robustness of **QR-Adaptor** is also evident, especially on tasks that typically cause performance degradation for other methods.

G.2 VISUALIZATION RESULTS FOR THE MMLU TASK

The results for the MMLU task in LLaMA2 are shown in Figure 2. **QR-Adaptor** demonstrates outstanding performance across various benchmarks. Due to the rank value selection ranging from 2 to 16, in some cases, **QR-Adaptor** consumes less memory than the fine-tuned 4-bit quantized models. Moreover, the low-precision models fine-tuned by **QR-Adaptor** outperform the fine-tuned 16-bit

1188

1189

1190

1191

1192

1193

**Table 8:** Performance comparison of different methods across various bit-width configurations on Llama2-13B. Superscripts on LoftQ bits indicate the number of initialization iterations. QR-Adaptor searches for optimal bit number and rank value for each layer based on different tasks with its bit number averaged across tasks. Bold figures represent the best performance for a given model and task, while underlined figures indicate the second-best. Accuracy is reported as %.

1194

1195

1196

1197

1198

1199

1200

1201

1202

1203

1204

1205

1206

1207

1208

1209

1210

1211

1212

1213

1214

1215

1216

1217

1218

1219

1220

1221

1222

1223

1224

1225

1226

1227

1228

1229

1230

1231

1232

1233

1234

1235

1236

1237

1238

1239

1240

1241

	Method	Bit	ARC(C)	ARC(E)	BoolQ	HellaS	OBQA	PIQA	WinoG	Average
Rank = 8	LoRA	16	<u>52.56</u>	<u>80.18</u>	81.44	<u>79.98</u>	<b>46.40</b>	<u>81.12</u>	71.98	<u>70.52</u>
	QLoRA	8	52.39	<u>80.18</u>	81.22	79.92	45.00	80.47	<b>73.09</b>	70.32
	QLoRA	4	51.54	78.91	81.41	79.46	45.40	80.30	71.82	69.83
	AdaLoRA	16	49.15	79.46	80.37	79.25	45.40	80.47	72.30	69.49
	AdaLoRA	8	49.32	79.34	80.43	79.29	45.60	80.47	72.22	69.52
	AdaLoRA	4	48.29	77.78	80.40	78.12	44.20	80.14	71.74	68.67
	LoftQ	4 <sup>1</sup>	50.68	78.79	81.16	79.12	<u>45.80</u>	80.41	71.35	69.62
	LoftQ	4 <sup>5</sup>	50.34	78.87	80.24	78.81	45.20	80.25	70.80	69.22
	LQ-LoRA	4	50.60	78.79	80.67	78.91	45.00	80.14	71.11	69.32
	<b>QR-Adaptor</b>	<b>6.125</b>	<b>52.82</b>	<b>80.64</b>	<b>81.84</b>	<b>80.08</b>	<u>45.80</u>	<b>81.45</b>	<u>72.69</u>	<b>70.76</b>
Rank = 16	LoRA	16	52.13	79.84	81.50	80.07	<b>46.20</b>	<u>81.23</u>	71.98	70.42
	QLoRA	8	51.54	<u>80.01</u>	81.13	79.86	<b>46.20</b>	81.18	72.22	70.31
	QLoRA	4	51.45	79.04	81.04	79.48	45.60	80.47	71.82	69.84
	AdaLoRA	16	49.40	79.34	80.46	79.28	45.40	80.47	72.30	69.52
	AdaLoRA	8	49.49	79.29	80.40	79.27	45.40	80.52	<u>72.38</u>	69.54
	AdaLoRA	4	48.29	77.69	80.43	78.10	44.20	80.09	71.67	68.64
	LoftQ	4 <sup>1</sup>	50.68	78.87	80.86	79.18	<u>45.80</u>	80.30	71.90	69.66
	LoftQ	4 <sup>5</sup>	50.60	78.96	80.92	79.15	45.40	80.41	71.59	69.58
	LQ-LoRA	4	50.09	78.79	80.43	79.06	45.40	80.14	71.67	69.37
	<b>QR-Adaptor</b>	<b>6.125</b>	<b>52.82</b>	<b>80.64</b>	<b>81.84</b>	<b>80.08</b>	<u>45.80</u>	<b>81.45</b>	<u>72.69</u>	<b>70.76</b>

models. Another advantage of the **QR-Adaptor** is that it can be implemented without any additional technical measures to optimize performance, apart from spending some time (about 15 minutes to get one data point). This simple but effective method is very useful in practical applications.

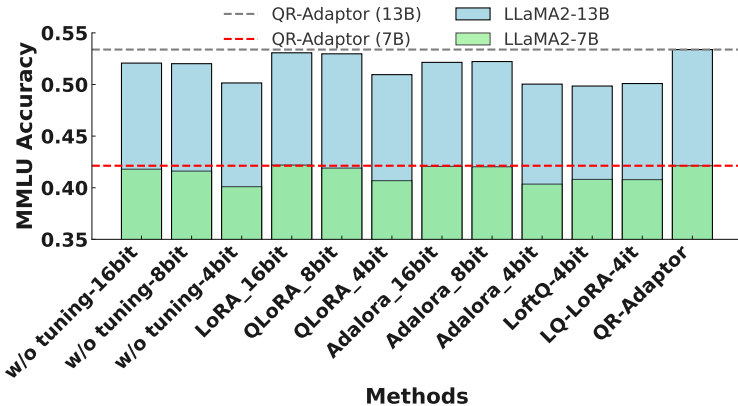


**Figure 2:** Performance comparison on MMLU benchmark. QR-Adaptor outperforms other methods.

### G.3 EFFECTIVENESS ON LARGER DATASETS WITH HIGHER RANKS

To address the concern regarding the effectiveness of small LoRA ranks on larger datasets, we conducted additional experiments on the LLaMA3.1-8B model using a larger dataset consisting of 177k samples. We tested our method with higher LoRA ranks (32 and 64) to evaluate its performance in handling large-scale data.

Our results are summarized in Table 9. The table compares the performance of **QR-Adaptor** with other baseline methods, including LoRA, QLoRA, AdaLoRA, and LoftQ, across various tasks. The

**Table 9:** Performance comparison of different methods across various bit-width configurations on Llama3.1-8B with higher ranks. Bold figures represent the best performance for a given model and task, while underlined figures indicate the second-best. QR-Adaptor\* is transferred config. Accuracy is reported as %.

Method	Rank	Bit	ARC(C)	ARC(E)	BoolQ	HellaS	OBQA	PIQA	WinoG	MMLU	Average
LoRA	32	16	54.86	82.74	82.75	<u>79.21</u>	44.40	<u>81.99</u>	74.11	63.66	70.47
LoRA	64	16	<u>55.46</u>	82.95	<u>82.94</u>	79.13	45.00	81.88	<u>74.51</u>	<u>64.34</u>	<u>70.78</u>
QLoRA	32	8	55.20	<u>83.12</u>	81.93	79.07	<b>46.20</b>	81.88	73.32	63.28	70.50
QLoRA	32	4	53.41	80.89	82.05	78.42	43.60	80.90	73.01	60.97	69.16
QLoRA	64	8	<u>55.46</u>	83.04	81.96	79.17	<u>45.80</u>	81.94	73.01	63.34	70.47
QLoRA	64	4	53.41	81.19	81.74	78.35	44.60	80.69	72.06	60.79	69.10
AdaLoRA	32	8	53.92	81.82	82.20	78.57	<b>46.20</b>	81.50	73.40	63.82	70.18
AdaLoRA	32	4	51.45	81.02	80.86	77.30	42.40	80.96	72.53	58.15	68.08
AdaLoRA	64	8	53.92	82.11	81.93	78.74	46.20	81.39	73.95	63.88	70.27
AdaLoRA	64	4	52.13	80.98	81.04	77.20	42.20	80.85	72.77	58.07	68.16
LoftQ	32	4 <sup>1</sup>	53.84	81.36	81.41	78.12	43.00	81.50	73.56	59.40	69.02
LoftQ	32	4 <sup>5</sup>	52.56	81.36	81.96	78.05	42.80	81.45	73.09	59.41	68.84
LoftQ	32	4 <sup>10</sup>	51.62	81.31	82.51	78.16	43.60	81.34	72.30	59.12	68.75
LoftQ	64	4 <sup>1</sup>	52.82	81.40	81.59	78.23	43.20	81.34	73.88	59.78	69.03
LoftQ	64	4 <sup>5</sup>	52.39	81.10	81.13	78.33	43.40	81.34	73.24	58.69	68.70
LoftQ	64	4 <sup>10</sup>	51.71	81.23	81.62	78.37	43.20	81.01	72.77	59.25	68.65
QR-Adaptor*	32	3.625	55.23	82.89	82.65	79.12	45.40	81.77	73.88	63.78	70.59
QR-Adaptor	32	5.875	<b>56.12</b>	<b>83.45</b>	<b>83.21</b>	<b>79.78</b>	<b>46.20</b>	<b>82.10</b>	<b>74.59</b>	<b>64.40</b>	<b>71.23</b>

performance metrics include accuracy scores on datasets such as ARC (Challenge), ARC (Easy), BoolQ, HellaSwag, OpenBookQA, PIQA, WinoGrande, and MMLU.

#### KEY OBSERVATIONS

- **Effectiveness of LoRA Initialization:** Despite using higher ranks (32 and 64) and larger datasets, methods like LoftQ and LQ-LoRA do not consistently outperform the standard QLoRA baseline or the quantized models without fine-tuning. Increasing iterations in LoftQ (from LoftQ-1 to LoftQ-10) to better fit quantization errors leads to performance degradation, especially on challenging tasks like MMLU and GSM8K. These results suggest that fitting quantization errors using LoRA initialization is not universally effective and may introduce noise that hinders model performance.
- **Effectiveness on Larger Datasets:** Our method, **QR-Adaptor**, consistently achieves superior performance across all tasks and outperforms other methods, confirming its robustness and scalability. The results validate that **QR-Adaptor** is effective even when small LoRA ranks might not suffice for larger datasets.
- **Impact of Adaptive LoRA Rank Reduction:** AdaLoRA exhibits performance drops, particularly with lower bit-widths and on more challenging tasks. This supports our observation that dynamically adjusting the rank during fine-tuning can lead to convergence issues in quantized models, which are less robust due to quantization errors.

These results reinforce our initial observations and highlight the limitations of methods that attempt to fit quantization errors through LoRA initialization. The inability of LoftQ and AdaLoRA to improve performance significantly, even with higher ranks and larger datasets, underscores the challenges associated with such approaches. In contrast, **QR-Adaptor**, guided by our proposed constraints, demonstrates consistent performance improvements.

#### G.4 FAIRER COMPARISON: MATCHING BIT-WIDTH CONFIGURATIONS

Another important consideration for a fair comparison of quantization methods is the bit-width configuration used. To ensure that prior methods are evaluated under the same conditions as QR-Adaptor, we have re-evaluated AdaLoRA and LoftQ using the same mixed-precision configurations that were optimized through QR-Adaptor’s framework. The updated results for Llama 2-13B are shown in Table 10.

The results indicate that the initialization constraints applied by QR-Adaptor provide substantial improvements over the original configurations of AdaLoRA and LoftQ. Despite these improvements, QR-Adaptor still outperforms these methods in terms of overall task performance. The constraints,



**Table 10:** Performance comparison with fair bit-width configurations for Llama2-13B. Accuracy is reported as %

Method	BoolQ	PIQA	HellaS	WinoG	ARC(E)	ARC(C)	OBQA	Average
AdaLoRA	81.08	80.13	79.21	71.74	79.51	50.12	45.60	69.77
LoftQ	80.93	79.47	79.02	71.34	79.26	51.20	45.60	69.98
QR-Adaptor	<b>81.84</b>	<b>81.45</b>	<b>80.08</b>	<b>72.69</b>	<b>80.64</b>	<b>52.82</b>	<b>45.80</b>	<b>70.76</b>

specifically ensuring stable initialization and fixing trainable parameters, contribute significantly to the enhanced performance of QR-Adaptor.

### G.5 IMPACT OF LONGER FINE-TUNING EPOCHS ON UNFIXED PARAMETERS

While increasing the fine-tuning epochs for AdaLoRA can lead to some performance improvements, these gains are marginal and AdaLoRA still does not outperform other methods like LoRA, QLoRA, or our proposed QR-Adaptor.

### FINDINGS

- **Marginal Improvement with Increased Epochs:** Extending the training of AdaLoRA from 2 epochs to 5 epochs results in a slight performance increase. However, this improvement is not substantial and comes at the cost of significantly longer training times.
- **Need for Mixed-Precision with Adaptive Rank:** The results suggest that adaptive rank adjustment alone, as in AdaLoRA, may not be the most effective approach. The combination of adaptive rank with mixed-precision quantization, as in QR-Adaptor, yields superior performance.

### SUPPORTING DATA

We provide an updated table below that includes an "Epochs" column, showing the results for LoRA, QLoRA, AdaLoRA (at 2 and 5 epochs), and QR-Adaptor.

**Table 11:** Performance comparison of different methods with varying fine-tuning epochs on Llama3.1-8B. Accuracy is reported as %

Method	Rank	Bit-width	Epochs	ARC (C)	ARC (E)	BoolQ	GSM8K (S)	GSM8K (F)	HellaS	OBQA	PIQA	WinoG
LoRA	8	16	2	56.14	83.88	83.18	54.36	54.28	79.44	45.20	82.10	<b>75.30</b>
QLoRA	8	8	2	57.08	83.46	82.48	53.75	53.90	79.63	<b>46.00</b>	82.10	74.59
QLoRA	8	4	2	54.35	82.41	82.08	44.35	44.50	78.82	44.20	81.50	73.64
AdaLoRA	8	16	2	52.90	81.99	81.87	50.57	50.57	78.65	45.00	81.34	73.95
AdaLoRA	8	16	5	53.50	82.25	82.05	51.00	50.90	78.75	45.20	81.40	74.10
AdaLoRA	8	8	2	52.90	81.86	82.05	49.96	49.96	78.65	44.80	81.34	74.43
AdaLoRA	8	8	5	53.10	82.00	82.10	50.20	50.10	78.70	45.20	81.38	74.50
AdaLoRA	8	4	2	51.28	80.98	80.61	37.83	38.36	77.36	42.80	80.74	72.53
AdaLoRA	8	4	5	51.50	81.10	80.75	38.00	38.50	77.40	43.20	80.78	72.60
QR-Adaptor	8	5.375	2	<b>56.83</b>	<b>84.12</b>	<b>83.38</b>	<b>56.29</b>	<b>56.11</b>	<b>80.93</b>	<b>45.80</b>	<b>82.92</b>	75.10

### OBSERVATION

- **AdaLoRA's Performance with Increased Epochs:** As observed, AdaLoRA shows only slight performance improvements when training is extended from 2 to 5 epochs. Even with the increase in epochs, AdaLoRA's performance does not surpass that of LoRA, QLoRA, or QR-Adaptor at 2 epochs.
- **QR-Adaptor's Consistency:** QR-Adaptor consistently achieves superior performance across all tasks, further validating the effectiveness of our method over other adaptive rank-based approaches.

- **16-bit AdaLoRA Performance:** Notably, AdaLoRA with 16-bit precision (not quantized) still underperforms compared to LoRA and QLoRA, suggesting that the adaptive rank mechanism alone is not enough, and the integration of mixed-precision quantization is crucial.

## G.6 IMPACT OF 2-BIT QUANTIZATION AND LOFTQ ITERATIONS

We have conducted additional experiments to explore the performance of LoftQ with 2-bit quantization and its variations across different numbers of iterations.

In these experiments, we used the NF2 variant from LoftQ, based on QLoRA’s NF4, to implement 2-bit quantization, since QLoRA does not natively support this low-bit quantization (as stated in the original paper and the GitHub repository). The 2-bit results in the LoftQ paper were also based on this NF2 variant. We fine-tuned the models using a 52k dataset, with the rank for LoftQ set to 16. The superscripts on LoftQ’s bit-width values represent the number of LoftQ iterations, with 0 iterations considered approximately equivalent to QLoRA (since QLoRA does not provide a 2-bit quantization type).

The results of our experiments are summarized in Table 12.

**Table 12:** Performance comparison for 2-bit quantization and LoftQ iterations on LLaMA3.1-8B with 52k fine-tuning dataset. Superscripts on LoftQ bits indicate the number of initialization iterations. Accuracy is reported as %

Method	Bit-width	MMLU	GSM8K	ARC(C)	ARC(E)	BoolQ	HellaS	OBQA	PIQA	WinoG
LoftQ	2 <sup>0</sup>	23.76	0.00	26.24	25.25	37.83	26.86	29.40	52.55	49.18
LoftQ	2 <sup>1</sup>	24.71	0.00	25.17	25.25	37.83	25.73	29.20	51.58	49.33
LoftQ	2 <sup>5</sup>	24.65	0.00	25.17	24.83	37.83	26.30	28.20	51.41	49.41
LoftQ	2 <sup>10</sup>	24.80	0.00	<b>26.02</b>	25.25	37.83	26.53	<b>29.80</b>	<b>52.83</b>	48.86
QR-Adaptor	3.625	<b>62.58</b>	0.53	<b>55.93</b>	<b>82.43</b>	<b>82.13</b>	<b>79.23</b>	<b>45.60</b>	<b>81.83</b>	<b>74.79</b>

## KEY OBSERVATIONS

- **MMLU Performance:** For the MMLU dataset, which involves multiple-choice questions, models with 2-bit quantization perform at approximately 25% accuracy, which is close to random guessing. Thus, LoftQ’s 2-bit quantization yields little practical improvement for MMLU on LLaMA3.1. This suggests that the performance of LoftQ with 2-bit quantization is not robust on complex tasks.
- **GSM8K Performance:** On the GSM8K dataset, LoftQ’s 2-bit quantization fails to provide any meaningful performance, resulting in 0% accuracy. This highlights the challenges of quantizing LLaMA3.1 to such low precision, especially on complex question-answering tasks.
- **Common Sense Reasoning Tasks:** For simpler reasoning tasks like WinoGrande, the LoftQ 2-bit quantized models show some capacity to answer, but there is no significant difference across LoftQ’s iterations, and the models still perform similarly to random guessing on most datasets.
- **QR-Adaptor Optimization:** For QR-Adaptor, we optimized based on theoretical memory savings from 4-bit quantization. Since 2-bit quantization does not reduce memory usage effectively, we used the theoretical savings in our optimization process. This optimization allowed QR-Adaptor to achieve better performance even when compared to LoftQ with 2-bit quantization.

## CONCLUSION

From these results, we observe that LoftQ’s 2-bit quantization shows poor performance across the board. Even with multiple iterations (up to 10), LoftQ struggles to achieve reasonable accuracy on tasks like MMLU and GSM8K. In contrast, QR-Adaptor, with its unified optimization of both rank and bit-width during fine-tuning, consistently outperforms LoftQ and other methods.

Notably, while LoftQ’s 2-bit quantization performs poorly, QR-Adaptor manages to retain much better performance by leveraging the advantages of mixed-precision quantization, making it a more effective solution for LLaMA3.1. These findings suggest that for models requiring high precision, such as LLaMA3.1, extreme quantization to 2-bit precision may not be viable, and more moderate bit-widths, as used by QR-Adaptor, provide better results.

We hope these results contribute to the ongoing discussions in the community regarding effective quantization strategies and provide further insights into the practical use of quantized models.

## H VERSION OF LLMS

We provide the Hugging Face link of LLMs used in the experiment: LLaMA2-7B: <https://huggingface.co/NousResearch/Llama-2-7b-hf>; LLaMA2-13B: <https://huggingface.co/NousResearch/Llama-2-13b-hf>; LLaMA3.1-8B: <https://huggingface.co/meta-llama/Llama-3.1-8B>.

## I MORE IMPLEMENTATION DETAILS

In optimizing the pruned Llama2-7B model, a carefully designed hyperparameter configuration has been implemented to strike a balance between model performance and computational efficiency. The model is fine-tuned using a learning rate of  $3 \times 10^{-4}$ , with a batch size of 128, divided into micro-batches of 4 to effectively manage memory limitations. Input sequences are capped at 256 tokens, and a dropout rate of 0.05 is applied to the LoRA layers, specifically targeting the query, key, value, and output projections, as well as the gate, down, and up projections. Layer-specific quantization is applied at both 4-bit and 8-bit levels, optimizing memory usage while maintaining computational accuracy. The training is performed using the paged AdamW optimizer with 32-bit precision, ensuring both stability and efficiency. These settings have been rigorously tested and refined through the Optuna framework to achieve an optimal balance between model performance and resource efficiency.

## J MORE ABLATION

We conducted comprehensive ablation studies to evaluate the impact of initialization metrics and the sensitivity of the proposed Pareto Ranking Genetic Algorithm (PRGA) to key hyperparameters, including iteration counts and population size. These experiments aim to further substantiate the effectiveness of our proposed approach.

### J.1 GRADIENT NORMS VS. RELATIVE ENTROPY

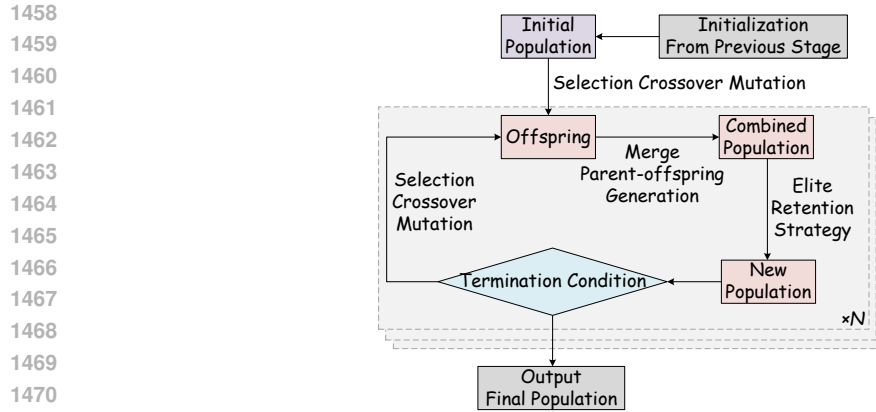
To assess the efficacy of initialization metrics, we compared the use of gradient norms and relative entropy in quantifying layer importance for fine-tuning quantized LLMs. The experimental results are summarized in Table 13.

**Table 13:** Comparison of gradient norms and relative entropy as initialization metrics on Llama2-13B. Bold values indicate the best performance for each task. Accuracy is reported as %

Initialization Metric	BoolQ	PIQA	HellaS	WinoG	ARC(E)	ARC(C)	OBQA	Average
Gradient Norms	80.79	80.13	79.16	71.69	78.72	50.97	45.40	69.51
Relative Entropy	<b>81.08</b>	<b>80.83</b>	<b>79.80</b>	<b>71.98</b>	<b>79.13</b>	<b>51.65</b>	<b>45.60</b>	<b>70.07</b>

### Insights:

- **Limitations of Gradient Norms:** Gradient norms exhibit limited variability and are prone to biases induced by quantization, which undermines their reliability as an initialization metric for quantized models.



1472 **Figure 3:** Detailed PRGA flow chart. The input is a set of solutions from the initialization, and the output is a  
1473 set of Pareto front solutions containing multiple solutions.

- 1474  
1475  
1476 • **Advantages of Relative Entropy:** Relative entropy captures task-specific layer importance  
1477 more effectively, resulting in robust initialization and improved performance in downstream  
1478 optimization.

1479  
1480 **J.2 SENSITIVITY TO ITERATION COUNTS AND POPULATION SIZE**

1481  
1482 To analyze the sensitivity of PRGA to hyperparameters, we systematically varied the number of  
1483 iterations and population sizes. Table 14 presents the results of these experiments.

1484  
1485  
1486 **Table 14:** Sensitivity analysis of PRGA under different iteration counts and population sizes on Llama3.1-8B.  
1487 Bold values indicate the best configuration.

1488  
1489

Iterations	Population Size	Average Improvement (%)	Total Time (min)
5	3	+0.8	72
5	5	+1.2	90
10	5	+1.5	135
5	20	+1.6	225
10	20	<b>+2.3</b>	270

1494  
1495 **Insights:**

- 1496  
1497 • **Trade-offs in Population Size:** Smaller population sizes (e.g., 3) reduce computational  
1498 cost but may fail to adequately explore the search space. Larger population sizes (e.g., 20)  
1499 improve exploration and convergence but increase computational overhead.
- 1500  
1501 • **Impact of Iteration Count:** Increasing the number of iterations improves optimization  
1502 quality, as reflected in better Pareto fronts. However, the marginal benefits diminish beyond  
1503 10 iterations, indicating limited practical gains for further increases.
- 1504  
1505 • **Balanced Configuration:** A population size of 5 and 5 iterations strikes a balance between  
1506 performance improvement and computational efficiency. This configuration can be adjusted  
1507 based on specific resource availability or performance requirements.

1508  
1509 **K VISUALIZATION OF OPTIMIZATION STAGES**

1510  
1511 Here we visualize Stage 2: Global Exploration with PRGA (in Figure 3) and Stage 3: Local  
Refinement with Bayesian Optimization (in Figure 4)

1512  
1513  
1514  
1515  
1516  
1517  
1518  
1519  
1520  
1521  
1522  
1523  
1524  
1525  
1526  
1527  
1528  
1529  
1530  
1531  
1532  
1533  
1534  
1535  
1536  
1537  
1538  
1539  
1540  
1541  
1542  
1543  
1544  
1545  
1546  
1547  
1548  
1549  
1550  
1551  
1552  
1553  
1554  
1555  
1556  
1557  
1558  
1559  
1560  
1561  
1562  
1563  
1564  
1565

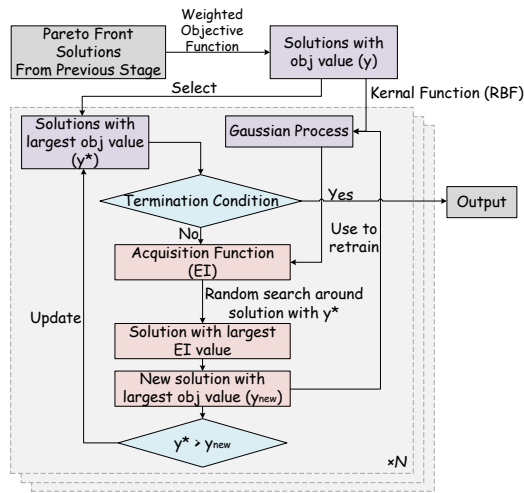


**Figure 4:** Detailed Bayesian optimization flow chart. Input is the Pareto front solution set from the global search, and output is a set of optimal solutions obtained according to the requirements.

## L LIMITATION

Compared to previous methods, the only additional cost is time, which is mainly introduced by testing on the calibration dataset. Although the configurations optimized on different datasets have a certain degree of portability, this limitation is reduced to some extent. In addition, we are studying some approximate methods to speed up the process.